LEVEL III

COMPOSITE PYROELECTRIC MATERIALS

FINAL TECHNICAL REPORT

1 Oct 79 - 30 Sep 80

October 1, 1979 to September 30, 1980

Contract Period October 1, 1979 to September 30, 1980

MDA903-78-C-0306, ARPA Order-3617

by

R.E. Newnham and A.S. Bhalla

Materials Research Laboratory
The Pennsylvania State University
University Park, Pennsylvania 16802

(814)865-1612

This research was sponsored by the Defense Advanced Research Projects Agency under ARPA Order No. 3617 Contract No. MDA903-78-C-0306 monitored by Lynn Garn, Night Vision and Electro-Optics Laboratory.

THE MATERIALS RESEARCH LABORATORY

THE PENNSYLVANIA STATE UNIVERSITY

UNIVERSITY PARK, PENNSYLVANIA

TABLE OF CONTENTS

		Page
I.	REPORT SUMMARY.	1
II.	COMPOSITE PYROELECTRIC MATERIALS.	2
	1. INTRODUCTION.	2
	2. COMPOSITES.	2
	a) PZT:Polymer	2
	b) Boracite:Polymer.	2
	c) Boracite:Lead Germanate	4
	d) Glass-Ceramics.	5
	3. SINGLE CRYSTALS	5
	a) Silicates and Germanates.	5
	b) Resorcinol.	6
	c) Antimony Sulfur Iodide (SbSI)	6
	4. INSTRUMENTATION	6

APPENDIX I. PYROELECTRIC PZT-POLYMER COMPOSITES

APPENDIX II. PYROELECTRIC $Li_2Si_2O_5$ GLASS-CERAMICS

APPENDIX III. $Ba_2TiGe_2O_8$ AND Ba_2O_8 PYROELECTRIC GLASS-CERAMICS

APPENDIX IV. PAPER PRESENTED AT THE AMERICAN CRYSTALLOGRAPHIC ASSOCIATION MEETING, MARCH 1980, ALABAMA

APPENDIX V. PYROELECTRICITY IN SbSI

APPENDIX VI. PRIMARY AND SECONDARY PYROELECTRICITY IN SINGLE CRYSTALS OF ANTIMONY SULPHUR IODIDE

APPENDIX VII. PAPER PRESENTED AT THE ACA MEETING, AUGUST 1980, CANADA

REPORT SUMMARY

This report describes work carried out in the Materials Research Laboratory of the Pennsylvania State University over the period October 1, 1979 to September 30, 1980 under DARPA Contract No. MDA903-78-C-0306. Under this program new types of composite materials and various single crystal materials are studied for pyroelectric applications. The pyroelectric figure of merit (p/K) has been measured using a fully automated direct (Byre-Roundy) and Chynoweth system built during the past year.

Composites of ferroelectric oxides such as PZT, boracites, lead germanate with the polymer spurrs were fabricated. In PZT-spurrs composites, the pyroelectric figure of merit p/K was improved by a factor of 7 over that of solid PZT. Boracites:Spurrs and Lead Germanate:Spurrs composites possess p/K values equivalent to the figure of merit of their respective single crystalline forms, (Appendix I).

A new technique has been developed to fabricate oriented glass-ceramic pyroelectric targets using large temperature gradients across the glass disk. Pyroelectric figures of merit (p/K) for recrystallized $Li_2Si_2O_5$, $Ba_2Ge_2TiO_8$ and $Ba_2Si_2TiO_8$ were up to 60% of the single crystal values, (Appendices II, III, IV).

Single crystals of antimony sulfur iodide, lithium silicate, lithium germanate, and resorcinol are studied for their potential applications in the pyroelectric devices. SbSI family members have some potentials as oblique-cut targets at low temperatures, (Appendices V, VI, VII).

COMPOSITE PYROELECTRIC MATERIALS

1. Introduction

This report describes work carried out in the Materials Research Laboratory of the Pennsylvania State University over the period Oetober 1, 1979 to September 30, 1980 under DARPA Contract No. MDA903-78-C-0306. Under this program, new types of composite materials were studied for pyroelectric applications and the pyroelectric figure of merit (p/K) has been measured by direct (Byer-Roundy) and Chynoweth methods. The important families of materials studied are described in brief in the following paragraphs and the detailed results in the published papers are attached as appendices.

2. Composites

a) PZT:Polymer

PZT-Spurrs composites fabricated by the replamine technique improves the pyroelectric figure of merit p/ε by a factor of 7 over that of solid PZT. The temperature dependence of the pyroelectric response exhibits an interesting compensation point where the primary and secondary effects cancel out. At room temperature the hard plastic mechanically elamps the PZT, but at higher temperatures the plastic softens. PZT-soft polymer composites showed no enhancement of the pyroelectric figure of merit. Major changes in the pyroeleetric response were noted when the sample thickness was compared to the scale of the composite heterogeneity.

The details of the sample preparations, measurements and the results are described in Appendix I.

b) Boracite:Polymer

Fe-I and Ni-Br boracite single crystal samples were obtained from Plessey Company. The tiny crystals were crushed and screened between 100 and 200 mesh

and then loaded in a thick Spurrs epoxy film. The films were polished to a thickness of 100 μm in an approximate 3:1 connectivity pattern. The composite films were poled in an electric field of 20 KV/cm. The following observations were made on these composites.

(1) In Fe-I boracite composites a strong pyroelectric signal was observed after poling in a field of 20 KV/cm for two minutes (Chynoweth method). The signal increased with successive polings at room temperatues.

(2) 100% reversal of the pyroelectric signal was observed when the field of 20 KV/cm was applied opposite to the direction in the first poling.

(3) Single crystals of Fe-I boracite gave scattered values of p and K. It was difficult to pole the crystals in many cases. Efficient poling could not be achieved in several crystals. Mechanical fractures and chemical inhomogeniety seemed to be the major problem. In the best crystal the pryoelectric signals were comparable to those of the fully poled composites at room temperature (approximately 1/3 $LiTaC_3$ and 1/8 TGS).

(4) Compared to other composites, Fe-I boracite samples poled rather easily, possibly because (i) the dielectric constant of boracite is about the same as that of polymer, (ii) boracite has twelve domain orientations (<110>), far more than most ferroelectrics, (iii) fracture during poling process is minimized, (iv) because of the smaller particle size, the degree of chemical homogeniety in the crystallites was higher.

(5) On heating the pyroelectric signal increased. Near 60°C the signal was unstable and very sharp spikes were observed at higher temperatures. The spikes may correspond to various transitions occurring

in Fe-I boracite particles differing slightly in chemical composition. This is quite possible since it is difficult to obtain chemical homogeniety in single crystals. In our composite samples the powder used was prepared from grinding the several single crystals of Fe-I boracite. Also the boracite have very high electrical conductivity near the transition and thus the overall conductivity of the composite is increased accordingly.

If Fe-I boracite composites were well behaved at high temperatures, a very high figure of merit could be achieved. In this way, large area composites for pyroelectric vidicon devices could be made without the necessity of growing large single crystals. The idea has been tested on lead germanate composites. Figures of merit as high as the single crystal values were observed up to a temperature 80°C.

(6) Ni-Br boracite composites did not give encouraging pyroelectric signals when tested in a similar way. Potentially the material has a higher figure of merit than that of Fe-I boracite, but there are severe problems of chemical inhomogenieties and fracture during poling.

c) Boracite:Lead Germanate

Boracite ceramics were prepared from a fine-grained powder of Fe-I boracite. The powder was mixed with 2 wt % lead germanate powder and pressed into thin disks. The disks were sintered at 750°C and 3500 psi argon pressure in a hot isostatic pressure vessel (HIP) for five minutes. High density ceramics of boracite were obtained with the HIP process, and the pyroelectric response was measured after poling in a field of 20 KV/cm. The magnitude of the signal was smaller than those obtained from composites. Effects, similar to those

obtained in boracite-polymer composites were observed when the samples were heated through the phase transition.

These experiments suggest the potential for broacite composites, but a better quality boracite is needed to prepare the composites.

d) Glass-Ceramics

Pyroelectric-piezoelectric $Li_2Si_2O_5$ $Ba_2TiGe_2O_8$, $Ba_2TiSi_2O_8$, SbSI glass ceramics have been prepared by crystallizing highly-oriented surface layers from stoichiometric glass compositions in a temperature gradient. The technique provides a method of fabricating large and inexpensive pyroelectric and piezoelectric devices. However, one difficulty with lithium disilicate pyroelectric glass ceramics was that thin targets (<200 μm) cut perpendicular to the growth direction (the polar c axis of $Li_2Si_2O_5$) were extremely fragile and could not be prepared routinely. Improvements in the mechanical properties of the recrystallized targets and the pyroelectric properties were noted when small amounts of ZnO were added to the melt.

$Ba_2TiGe_2O_8$ and $Ba_2TiSi_2O_8$ glass-ceramics have physical properties superior to $Li_2Si_2O_5$ such that thin sections less than 100 μm in thickness can easily be prepared. Pyroelectric responses up to 50% of the single crystal values were observed because of the high degree of orientation of the crystallites in the glass-ceramic samples.

The work on glass-ceramics is described in Appendices II, III and IV.

3. Single Crystals

In addition to the composites, several other materials with large pyroelectric coefficients have been studied in single crystal form.

a) Silicates and Germanates

Lithium germanate and hemimorphite (zinc silicate) are attractive materials

for pyroelectric measurements. Single crystals of lithium germanate were grown by Czochralski pulling technique and good quality single crystals of hemimorphite were selected from the natural sources. A pyroelectric response (p/K) as high as 80% of lithium tantalate was observed in these materials. Though these materials have figures of merit only half that of TGS, they are easy to handle and prepare in the form of thin targets. Low density, low dielectric constant, and low dielectric losses make them attractive.

b) Resorcinol

Single crystals of resorcinol were grown from the water solution of resorcinol by slow evaporation method at 30°C. Inclusion-free crystals of large area were selected for the pyroelectric measurements. A pyroelectric figure of merit (p/K), as high as TGS was obtained at room temperature, but the resorcinol crystals are very sensitive to the atmospheric humidity, and are not a good replacement for TGS.

c) Antimony Sulfur Iodide (SbSI)

Single crystals of SbSI were grown by Bridgman and vapor growth techniques. Large pyroelectric coefficients were measured on these crystals, as described in Appendices V, VI and VIII.

4. Instrumentation

A fully atuomated Byre-Roundy experiment for measuring pyroelectric coefficients and their temperature dependence has been built, and is now in a routine use. Simultaneous measurements of dielectric constant can be made and the pyroelectric figure of merit (p/K) evaluated at temperatures ranging from liquid nitrogen to 200°C. The system has been tested with several standard materials for reliability and reproducibility.

Construction of a fully automated Chynoweth system for measuring the p/C_v and p/KC_p is underway (C_p = specific heat).

APPENDIX I

PYROELECTRIC PZT-POLYMER COMPOSITES

A. S. Bhalla, R. E. Newnham, L. E. Cross and W. A. Schulze

PYROELECTRIC PZT-POLYMER COMPOSITES

A. S. BHALLA, R. E. NEWNHAM, L. E. CROSS and W. A. SCHULZE

Materials Research Laboratory, The Pennsylvania State University, University Park, Pennsylvania 16802

and

J. P. DOUGHERTY† and W. A. SMITH

North American Philips, Briarcliff Manor, New York 10510

(Received July 30, 1980; in final form January 5, 1981)

PZT-Spurrs composites fabricated by the replamine technique improves the pyroelectric figure of merit p/ϵ by a factor of 7 over that of solid PZT. The temperature dependence of the pyroelectric response exhibits an interesting compensation point where the primary and secondary effects cancel out. At room temperature the hard plastic mechanically clamps the PZT, but at higher temperatures the plastic softens. PZT-soft polymer composites showed no enhancement of the pyroelectric figure of merit. Major changes in the pyroelectric response were noted when the sample thickness was comparable to the scale of the composite heterogeneity.

1 INTRODUCTION

Pyroelectric materials are of interest in thermal device applications[1] such as thermal image systems (vidicons), forest fire mapping, surveillance, burglar alarms, medical thermography, testing semiconductor integrated circuits, and energy-saving applications (locating heat losses in homes and factories). Presently, many of these devices are made either from pyroelectric single crystals or from ceramic discs of ferroelectric materials. In some of these applications large target materials are desirable. The availability of such targets is generally restricted by the size and expense of the single crystals, and by the low figure of merit of alternative materials. In terms of materials parameters the figure of merit is defined as

$$M_p = \frac{p}{\epsilon CD} \qquad (1)$$

where p, ϵ, C and D are the pyroelectric coefficient, the dielectric constant, the volume specific heat, and the lateral thermal diffusivity. In order to develop more efficient devices, an improvement in the figure of merit of pyroelectric materials is desirable so that the need for large single crystals can be relaxed. Recently, it has been demonstrated that piezoelectric composites made of PZT : polymer have piezoelectric g_{33} and g_h coefficients more than an order of magnitude higher than the coefficients of the homogeneously poled ferroelectric ceramics.[2-4] In this paper we report the fabrication of several PZT composites and compare their pyroelectric performance with normal PZT ceramics.

2 THEORETICAL MODELING

Under stress-free conditions, the measured pyroelectric coefficient is the sum of the primary and the secondary effect (product of thermal expansion, piezoelectric and elastic coefficients). For most ferroelectric materials, the primary and secondary coefficients are of opposite sign, lowering the overall pyroelectric response.[4] Clearly, if the piezoelectric response could be modified by suitable clamping, the secondary contribution to the pyroelectic effect can be altered. Thus, by fabricating a diphasic material with an appropriate second component, the pyroelectric coefficient can be changed significantly. It is suggested on the

† Present address: Gulton Industries, 212 Durham Avenue, Metuchen, NJ 08840.

basis of the following models that two-phase composites with suitably chosen modes of phase interconnection[2] (connectivity) can have property combinations that improve the figure of merit for device applications beyond those possible with the individual phases.

2.1 *Simple Series and Parallel Connection*

Consider the response of a multilayer diphasic pyroelectric (Figure 1a) made from a volume fraction ${}^1v$ of phase with permittivity ${}^1\epsilon_{33}$ and pyroelectric coefficient ${}^1p_3$, interleaved along the x_3-direction with a phase of volume fraction ${}^2v$, permittivity ${}^2\epsilon_{33}$, and pyroelectric coefficient ${}^2p_3$. Piezoelectric and thermal expansion coefficients are represented by d_{ij} and α_i, respectively. To simplify the calculation we assume that both phases are poled ceramics with conical symmetry and with the polar axis (x_3) perpendicular to the plane of the interleaving layers.

With close transverse connections of thin sheets, and assuming no surface tractions, the total pyroelectric effect ($\bar{p}_3$) is calculated for a uniform temperature change ΔT. There are two terms corresponding to the primary (sum of the primary and secondary effects, i.e., the net total pyroelectric effects of the pure phases) and secondary effects of the composite:

$$\bar{p}_3 \quad \frac{{}^1v\,{}^1p_{33}\,{}^2\epsilon_{33} + {}^2v\,{}^2p_3\,{}^1\epsilon_{31}}{{}^1v\,{}^2\epsilon_{33} + {}^2v\,{}^1\epsilon_{33}} + \frac{2\,{}^1v\,{}^2v({}^2\epsilon_{33}\,{}^1d_{31} - {}^1\epsilon_{33}\,{}^2d_{31})({}^2\alpha_1 - {}^1\alpha_1)}{({}^1v\,{}^2\epsilon_{33} + {}^2v\,{}^1\epsilon_{33})[{}^1v({}^2s_{11} + {}^2s_{12}) + {}^2v({}^1s_{11} + {}^1s_{12})]} \tag{2}$$

The corresponding electric permittivity is

$$\bar{\epsilon} = \frac{{}^1\epsilon\,{}^2\epsilon}{{}^1v\,{}^2\epsilon + {}^2v\,{}^1\epsilon} \tag{3}$$

The voltage coefficient is ratio of the pyroelectric coefficient and permittivity.

$$\frac{\bar{p}_3}{\bar{\epsilon}_{33}} = \frac{{}^1v\,{}^1p_3}{{}^1\epsilon_{33}} + \frac{{}^2v\,{}^2p_3}{{}^2\epsilon_{33}} + \frac{2\,{}^1v\,{}^2v({}^2\alpha_1 - {}^1\alpha_1)}{[{}^1v({}^2s_{11} + {}^2s_{12}) + {}^2v({}^1s_{11} + {}^1s_{12})]} \times \left(\frac{{}^1d_{33}}{{}^1\epsilon_{33}} - \frac{{}^2d_{31}}{{}^2\epsilon_{33}}\right). \tag{4}$$

The secondary pyroelectric effect of composit arises from thermal expansion mismatch (${}^2\alpha_1 - {}^1\alpha_1$). Because of the third term in Fq. (4) a pyroelectric effect can appear, even when ${}^1p_3 = {}^1p_3 = 0$. This is a good example of a product property since neither phase is required to exhibit primary pyroelectricity.

Secondary pyroelectric effects also appear in a composite with parallel connectivity (Figure 1b). In this case, the composite pyroelectric coefficient is

$$\bar{p}_3 = {}^1v\,{}^1p_3 + {}^2v\,{}^2p_3 + \frac{{}^1v\,{}^2v({}^2\alpha_3 - {}^1\alpha_3)({}^1d_{33} - {}^2d_{33})}{{}^1v\,{}^2s_{33} + {}^2v\,{}^1s_{33}} \tag{5}$$

and the permittivity is given by

$$\bar{\epsilon} = {}^1v\,{}^1\epsilon + {}^2v\,{}^2\epsilon. \tag{6}$$

In many pyroelectric (and piezoelectric) applications, low permittivity is very desirable. This is a problem in working with ferroelectric materials with large dielectric constants. To maximize the figure of merit, it would be very helpful to decouple the pyroelectric coefficient from the permittivity. In essence, this means changing form parallel to series connection during the processing

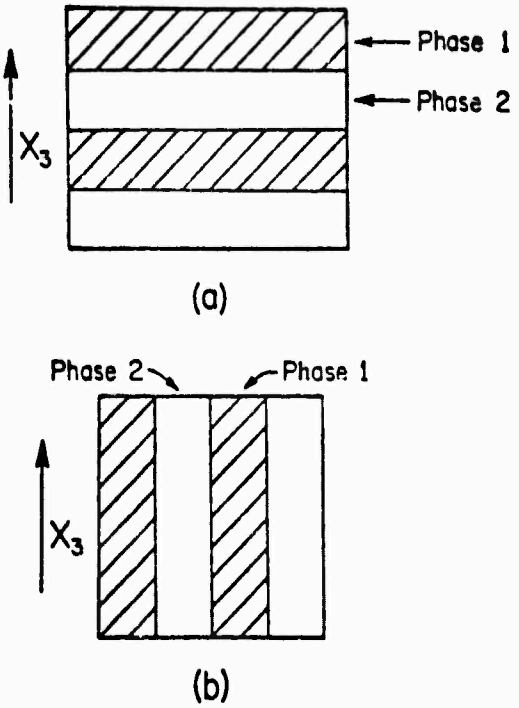

FIGURE 1 The series (a) and parallel (b) models used in estimating the piezoelectric and pyroelectric effects of diphasic solids.

steps, and keeping the pyroelectric effect large by making use of the secondary effect which acts through the piezoelectric coefficients and thermal expansion.

2.2 *Thermal Conduction*

Thermal diffusion causes a crosstalk problem in some pyroelectric device applications, such as vidicons operated at slow panning speeds.[1] Diffusivity is measured by heating one portion of the pyroelectric target and monitoring the electrical response at a position some distance away. Low thermal conductivity within the target is desirable in this regard. Triglycine sulfate and triglycine fluoberyllate are good insulators, but further improvement may be possible with composites. Essentially, this makes use of the reticulation principle proposed by Singer and Lalak.[1] Photolithography followed by etching is used to divide the target into a number of thermally-isolated islands.

The thermal conductivity coefficient k_{ij} relates heat flow to thermal gradient, $h_i = k_{ij}(\partial T/\partial x_j)$. In cubic crystals as well as in amorphous and polycrystalline materials, k_{ij} is a scalar so that thermal conduction is isotropic. This is not true for crystals having symmetry lower than cubic, nor is it true for anisotropic composites. Thermal conductivity is a second-rank tensor for composites with series or parallel connection, with principal axes parallel and perpendicular to the layers. By choosing two components with vastly different thermal conductivities (k values range over about five orders of magnitude), it is possible to incorporate enormous thermal anisotropy in a layered composite. Heat shields are an example. By way of comparison, with the best single phase materials, graphite conducts heat only four times better in the carbon layers than in the perpendicular direction.

2.3 *Modification of Electrical Conductivity*

Control of the electrical conductivity could also be accomplished in either the active or inactive component of the pyroelectric composite. Components of interest in this regard are photopolymers, thermopolymers, and ovonic glasses in which conductivity changes occur under irradiation, or by heating, or under electric fields. By altering the resistivity, build-up charge on the pyroelectric vidicon target surface could be leaked off.

3 PZT AND PZT:POLYMER COMPOSITES

3.1 *Materials*

To test some of these ideas we have investigated the pyroelectric characteristics of PZT:polymer composites. The two phases which have been used for the majority of these studies are a commercial PZT (Ultrasonic PZT 501†), and a 'hard' plastic casting component ('SPURRS'). The PZT 501 is a proprietary piezoelectric formulation, categorized as a 'soft' donor-doped material used primarily for its high piezoelectric d coefficients. It is ***not*** an optimum composition for pyroelectric response, but is a very easy formulation with which to reproduce consistent electrical properties. It appeared well suited to the modeling of composites for pyroelectric evaluation, where the changes in response affected by the composite are of primary interest, rather than the absolute levels.

SPURRS is a complex polymer system which has been developed primarily for casting and replication. It is a multicomponent system‡ in which the mechanical and thermomechanical properties can be controlled by adjusting the chemistry and curing temperature. A major advantage of this plastic for the replamine replication work is that the unpolymerized liquid has very low viscosity (60 cps), allowing good vacuum impregnation and a close mating of ceramic:plastic phases in fine-scale replications.

3.2 *Sample Preparation*

The following samples were prepared.

(*1*) *Pure Ultrasonic PZT 501.* Disk-shaped samples of the 501 formulation were prepared by cold pressing the powder and firing under controlled PbO partial pressure. Samples 1 cm diameter and 1 mm thick were fabricated. Sputtered chrome-gold electrodes were applied to the

---

†Ultrasonics Powders Inc., 2383 S. Clinton Ave., South Plainfield, NJ 07080.

‡SPURRS: A typical chemical mixture of the following chemicals in the gravimetric ratios:

RD-4 (VCD)	10 gm
D.E.R. 736	4 gm
NSA (nonethyl Succinic) anhydride	26 gm
DMAE (dimethyl amino ethanol)	0.4 gm

Setting time: 8 hours, 70°C.
Source: Ernest F. Fullam, Inc., Schenectady, NY 12301.
dielectric constant ≈4, density ≈1.1 gm/cm³.

major faces, and the ceramics poled under 14 *kv*/cm at 90°C for 5 minutes.

Completion of the poling was established by checking the piezoelectric coefficient d_{33} against standard samples. For pyroelectric study, samples were thinned to 200 μm by grinding and repolishing; after thinning, all samples were repoled and again checked for consistency of d_{33}.

(*2*) *PZT-Polymer Films.* Poled PZT 501 was ground to a fine powder, then classified to 400 mesh. The powder was then suspended in liquid monomer and the mixture dispersed on a teflon plate to form a thin layer. After curing at 70°C for 8 hours, samples were polished to a thickness of 35 μm and poled. The PZT-polymer ratio and the size distribution of PZT particles were determined by optical microscopy.

(*3*) *PZT-Polymer Replamine Samples.* Replamine samples were prepared using two coral species, porites goniopera and porites-porites.[2,3] The porites-porites has a dominantly 3:1 connectivity and were preferred for the replication experiments. Coral templates having a narrow pore size distribution, were used in making the PZT replica. Using a lost wax method,[3] porous PZT specimens of suitable dimensions were prepared from the templates. Soft polymer adiprin and the hard Spurrs were used for filling the PZT replicas in most of the samples. Variations in hardness of the Spurrs were achieved by altering the polymer composition and curing temperature.

4 ELECTRICAL MEASUREMENTS

In the present studies, emphasis has been placed upon the determination of the parameters $\bar{p}$ and $\bar{\epsilon}$, the effective average pyroelectric and dielectric constants for the composites, and the resulting ratio $\bar{p}/\bar{\epsilon}$. Qualitative pyroelectric response was evaluated by the Chynoweth method.[6] Automated quantitative measurements of the pyroelectric coefficients were made by the Byre-Roundy direct method.[7]

Dielectric properties were measured at both 1 MHz and 1 KHz. Although the 1 MHz dielectric data provide a better signal-to-noise ratio in the pyroelectric tests, possible piezoelectric resonances nearby in frequency make a 1 KHz dielectric measurement also necessary. For a 755 μm thick PZT 501 disk the permittivity at 1 MHz was found to be 60% of the 1 KHz value. The replamine composites, on the contrary, showed less than 10% dispersion, indicative of the damping effects of the second phase.

5 RESULTS AND DISCUSSION

5.1 *Pure Ultrasonics 501 PZT*

Samples were measured with as-fired surfaces electroded with air drying silver paste and also with polished surfaces electroded with sputtered gold-palladium. No significant differences were found for the two types of electrode. The dielectric constant was found to be quite sensitive to the degree of poling, showing the highest values in the electrically or thermally depoled state, often dropping by 25% after poling.

When samples were poled at high temperatures and held under dc bias while being cooled to room temperature, the initial heating cycle often showed anomalously large discharge currents originating from thermally-stimulated current (TSC). All graphs of p versus T are for data that were reproducible on temperature cycling.

A base line for the PZT composite system are the properties of pure PZT 501 (Figure 3).

$$p = 5 \times 10^{-4}\ \text{C/m}^2 - \text{K}$$
$$\epsilon \simeq 1800$$
$$p/\epsilon = 2.7 \times 10^{-7}\ \text{C/m}^2 - \text{K}$$

5.2 *PZT: Loaded Film*

The controlled grit size (35 μm) composite called a "loaded film" has the pyroelectric response of a dilute, pure PZT. The magnitude and temperature dependence of $\bar{p}/\bar{\epsilon}$ are very close to that of the solid PZT disc, while $\bar{p} \simeq 5 \times 10^{-5}\ \text{C/m}^2 - \text{K}$ and $\bar{\epsilon} \simeq 200$ are both reduced by a factor of ten.

5.3 *Replamine Composites*

a) PZT-Adiprin. Using the soft plastic, Adiprin, the measured pyroelectric values for the composites are

$$\bar{p} \simeq 2.25 \times 10^{-5}\ \text{C/m}^2 - \text{K}$$
$$\bar{\epsilon} \simeq 65\ (1\ \text{MHz})$$
$$\bar{p}/\bar{\epsilon} \simeq 3.5 \times 10^{-7}\ \text{C/m}^2 - \text{K}.$$

The temperature dependences are shown in Figure 2. The figure of merit, $\bar{p}/\bar{\epsilon}$, shows a slight im-

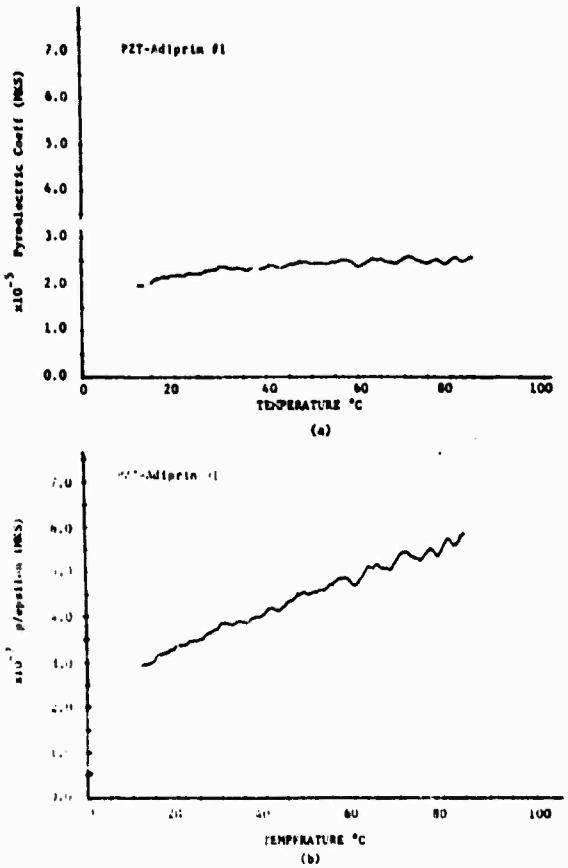

FIGURE 2 (a) pyroelectric coefficient and (b) figure of merit p/ϵ of PZT-Adiprin replamine composite of 6 mm thickness (absolute values of p).

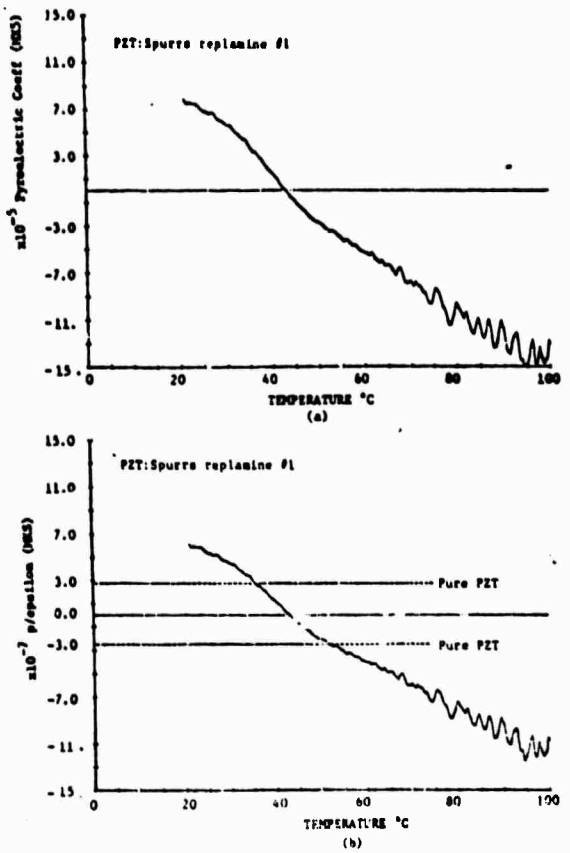

FIGURE 3 (a) pyroelectric coefficient and (b) figure of merit p/ϵ of PZT:Spurrs replamine composite: thickness 3 mm. p/ϵ for the pure PZT is shown for comparison in (b).

provement over the PZT because of a greater reduction of ϵ compared to p.

b) PZT-Spurrs Replamine. The pyroelectric behavior of two replamine PZT-Spurrs composites was measured. The first sample (3 mm thick) showed unusual pyroelectric behavior. As shown in Figure 3, the sign of the pyroelectric reverses at 45°C. The reversal of $\bar{p}$ was a reproducible effect over ten temperature cycles. The dielectric constant was reduced from the PZT values, as expected for the replamine composite, producing an improved figure of merit $\bar{p}/\bar{\epsilon}$ for temperatures well above or well below 45°C. The improvement in $\bar{p}/\bar{\epsilon}$ at $T \simeq 100$°C is nearly a factor of five.

A thinner 0.75 mm replamine sample of PZT:Spurrs was also measured. The pyroelectric data are shown in Figure 4. In contrast to the previous data on the PZT-Spurrs composite #1, these data showed no reversal in the sign of $\bar{p}$ (down to −10°C) and the figure of merit $(\bar{p}/\bar{\epsilon})$ was inferior to the pure PZT at room temperature.

The difference in the data could be produced in several ways including: (i) difference in the microstructure of the coral making up the samples; (ii) existence of a critical sample size with respect to the basic microstructural unit of the composite.

Comparison of the microstructures of the PZT-Spurrs samples shows no significant difference in the coral matrice. The basic microstructure unit in the two samples is 100–150 μm. The large microstructural unit suggests a critical dimension with respect to normal sample thicknesses. The sample showing a change in sign of $\bar{p}$ was 3 mm thick, whereas the sample without a crossover was 0.75 mm thick.

The 3 mm PZT:Spurrs sample was thinned to 2, 1, and then 0.5 mm. At each stage the microstructure was examined and a full set of pyroelec-

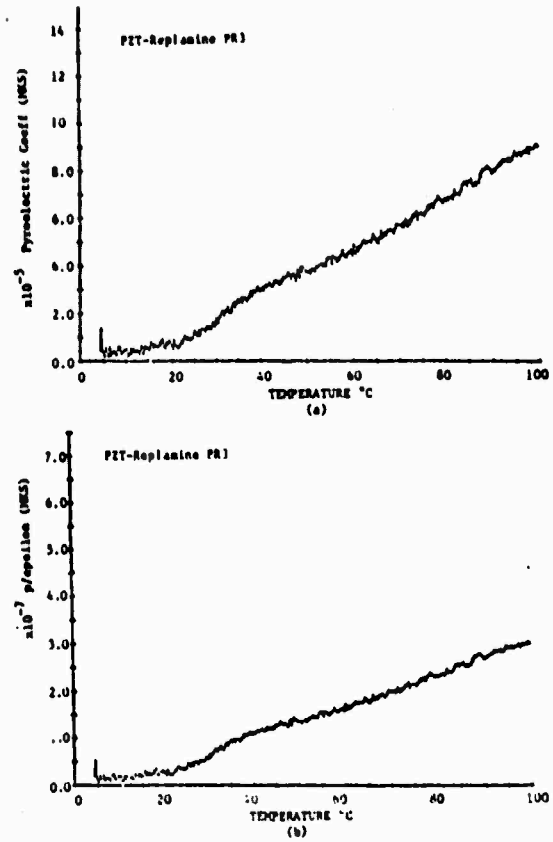

FIGURE 4 (a) pyroelectric coefficient and (b) figure of merit p/ϵ for a thin (0.7 mm) PZT : Spurrs replamine composite (absolute values of p).

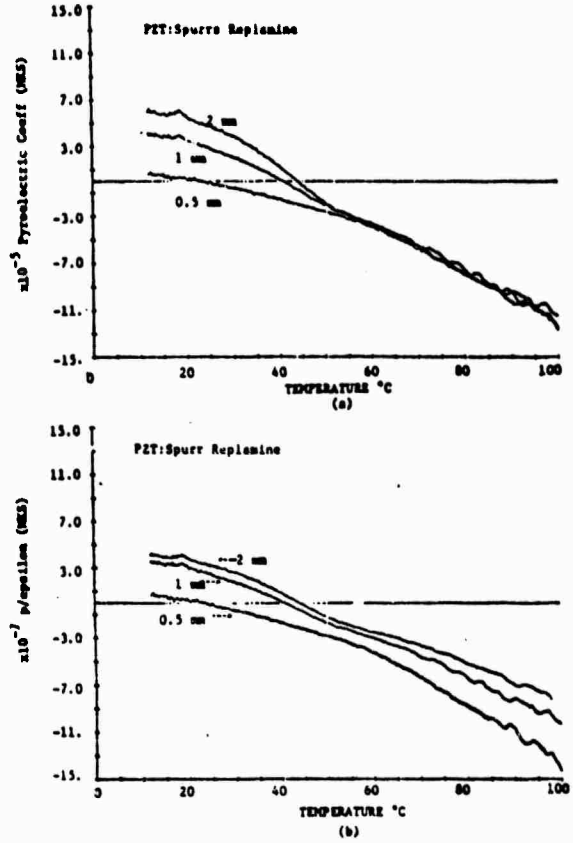

FIGURE 5 Thickness dependence (a); pyroelectric coefficient and (b) figure of merit p/ϵ of PZT : Spurrs replamine composite of 100–150 μm basic structural unit.

TABLE I

Pyroelectric Figure of Merit of PZT Based Composites

Sample	p $Cm^{-2}{}^{o}K^{-1}$ ($\times 10^{-4}$)	ϵ_r	p/ϵ, $Cm^{-2}{}^{o}K^{-1}$ ($\times 10^{-7}$)	Temperature (°C)	$(\bar{p}/\bar{\epsilon})$ composite / $(\bar{p}/\bar{\epsilon})$ PZT ceramic
Pure PZT-501	−5.0	1800	2.7–2.0	20	
Loaded film	−0.4	200	2.0	100	1.0
PZT-Adiprin	−0.225	65	3.5	20	1.3
PZT-Spurrs (PR-3)	−0.9	300	3	100	1.5
	−0.1	260	0.5	20	0.2
PZT-Spurrs (#1)	+0.8	130	6.0	25	2.2
3.0 mm thick	−1.5	120	11.0	100	5.5
2.0 mm thick	−1.2	130	8	100	4.0
1.0 mm thick	−1.2	100	11	100	5.5
0.5 mm thick	−1.2	80	14	100	7.0

tric data measured. The microstructure was found to be homogeneous through the thickness. However, a thickness dependence in the pyroelectric behavior was observed as shown in Figure 5. Data for the 3 mm thickness are not shown since the 2 mm data were essentially identical. While the details of the thickness behavior are not well understood, several important points emerge from the data:

1. Critical size effects show up for thicknesses as large as 6–10 microstructural units (the 1 mm sample).

2. For thicknesses of 3–5 microstructural units (the 0.5 mm sample), the qualitative behavior of p versus T differs from thicker samples.

3. For both regimes of thickness, samples show pyroelectric figures of merit ($\bar{p}/\bar{\epsilon}$) higher than the single phase material.

Measurements of $\bar{p}$, $\bar{\epsilon}$, $\bar{p}/\bar{\epsilon}$, and the comparative values of these composites to pure PZT are summarized in Table I. The pyroelectric response of the composites often show a sign reversal of the pyroelectric coefficient. Also, the magnitude of the pyroresponse decreases with the thickness at lower temperatures, but at high temperatures, the values for all the thicknesses are about the same. This behavior can be explained on the basis of Eq. (5) for the parallel connection model.

In the present composites the PZT and polymers are approximately in the 40% and 60% volume ratios. Taking the respective values of the constants for the two phases as

$$\begin{aligned}
\text{PZT} \quad & {}^1v = 0{\cdot}40 \\
& {}^1d = 400 \times 10^{-12}\ C/N \\
& {}^1s = 18 \times 10^{-12}\ \frac{m}{N^2} \\
& {}^1\alpha = 10^{-6}/°C \\
\text{Polymer} \quad & {}^2v = 0{\cdot}60 \\
& {}^2d = 0 \\
& {}^2s = 80 \times 10^{-12}\ \frac{m}{N^2} \\
& {}^2\alpha = 10^{-4}/°C
\end{aligned}$$

and substituting these numbers in the secondary contribution of Eq. (5), gives a value of $P_{sec} = +228\ \mu C/m^{2\circ}C$. The total pyroelectric effect from composite at room temperature thus should be

$$\begin{aligned}
P_T &= {}^1v\,{}^1p + 228 \\
&= +28\ \mu C/m^{2\circ}C.
\end{aligned}$$

The sign of the pyroelectric coefficient of the composite at room temperature is opposite to the total pyroelectric coefficient of pure PZT. At room temperature the polymer mechanically clamps the PZT, but at higher temperatures the polymer softens, reducing the clamping effect, and hence the secondary pyroelectric effect caused by thermal expansion mismatch in the composite. At sufficiently high temperatures the secondary effect is very small, since the clamping is minimal and the major contribution is then from the primary part. This also suggests that the thickness effect should disappear at higher temperatures. This is clearly seen in Figure 5. In this sample the composite secondary effect almost cancels the primary effect and as the temperature rises the primary effect takes over. Also in case of the adiprin PZT composite, clamping is very small, thus the secondary contribution is negligible and the pyroelectric response is essentially the primary part and the sample behaves as a dilute-d PZT system. Major changes were also noted when the sample thickness was comparable to the scale of the composite heterogeneity. Table I thus shows the enhanced $\bar{p}/\bar{\epsilon}$ over the pure PZT by a factor of 5 to 7 on the dominant 3:1 connectivity samples.

There are also additional advantages of a composite target material. If a polymer is employed as the host material, the target would be stronger and more flexible than a ferroelectric single crystal. Improvements in the density, specific heat and lateral thermal diffusivity are also expected.

SUMMARY

It is demonstrated that (i) In PZT-SPURRS composites fabricated by the replacmine process in dominant 3:1 connectivity, the simple pyroelectric figure of merit $\bar{p}/\bar{\epsilon}$ can be enhanced by a factor of 5 to 7; (ii) The data support the original hypothesis that the mode of phase interconnection is critical to the mechanism of enhancement in that the PZT Spurrs composites and PZT-soft polymer (adiprin) composites do not exhibit com-

parable properties; (iii) The scale of microstructure with respect to the smallest sample dimension can make a major change in the response.

ACKNOWLEDGEMENT

We wish to thank our colleagues at the Mat.rials Research Laboratory for their advice and assistance. This work was sponsored by the Defense Advanced Research Projects Agency (Contract DARPA Project P-15124-MS).

REFERENCES

1. B. Singer, *Advances in Image Pick Up and Display*, edited by B. Kagan (Academic Press, NY, 1977).
2. R. E. Newnham, D. P. Skinner and L. E. Cross, *Mat. Res. Bull.*, **13**, 525 (1978).
3. D. P. Skinner, R. E. Newnham and L. E. Cross, *Mat. Res. Bull.*, **13**, 599 (1978).
4. R. E. Newnham, L. J. Bowen, K. A. Klicker and L. E. Cross, *Mats. in Engg.*
5. A. S. Bhalla and R. E. Newnham, *Phys. Stat. Solidi.* (a) **58**, K19 (1980).
6. A. G. Chynoweth, *Phys. Rev.*, **102**, 705 (1956).
7. R. L. Byer and C. B. Roundy, *Ferroelectrics*, **3**, 333 (1972).

APPENDIX II

Pyroelectric $Li_2Si_2O_5$ Glass-Ceramics

G. J. Gardopee, R. E. Newnham, A. S. Bhalla

Pyroelectric $Li_2Si_2O_5$ Glass-Ceramics

G.J. Gardopee*, R.E. Newnham, A.S. Bhalla
Materials Research Laboratory
The Pennsylvania State University
University Park, Pennsylvania 16802

ABSTRACT

Highly oriented surface layers of lithium disilicate crystals were grown by crystallizing glasses of the composition $Li_2O:SiO_2$. The thickness of the oriented layer was a function of the thermal treatment. The crystallites in these layers were oriented with their c-axes perpendicular to the sample surface. These layers were found to be pyroelectric as determined by the Chynoweth technique. The pyroelectric responses of the glass-ceramics crystallized in a thermal gradient were approximately four times larger than that of a tourmaline crystal of similar dimensions.

---

*Present address: Perkin Elmer Corporation
100 Wooster Heights Road
Danbury, CT 06810

1. INTRODUCTION

The improvement of existing pyroelectric materials and the development of new pyroelectric materials with properties that are superior to those materials which are currently used, have been the goal of much of the research in the field of pyroelectrics. In the area of vidicon targets, these efforts have led to the development of deuterated triglycine fluoroberyllate (DTGFB). The ferroelectric crystals such as TGS and DTGFB require careful preparation and are subject to performance degradation due to depoling. The object of the present work was to crystallize a non-ferroelectric pyroelectric phase from a relatively simple oxide glass in a manner which would yield a composite with a pyroelectric response of a useful magnitude.

The concept of crystallizing an electrically active phase from an oxide glass has been employed in the past by the electronic materials industry. Extensive research at Corning Glass Works was directed towards developing a glass system from which $BaTiO_3$ could be crystallized to yield a high permittivity glass ceramic[1].

Electro-optic effects have been reported in glass-ceramics containing sodium niobate[2]. The optical properties of glasses containing crystallites of both sodium potassium niobate and barium titanate were studied for possible use as optical switching elements[3].

Layton and Smith[4] reported pyroelectricity in glass-ceramics in which the crystalline phase was ferroelectric. In this study, glasses containing crystals of $Na_{0.9}Cd_{0.5}NbO_3$ were poled. Reversible polarization and pyroelectricity were measured in their samples.

Reversible pyroelectricity has been reported in lithium niobate and lithium tantalate glasses[5]. This effect was explained as the result of ferroelectricity in the glassy state, but the possibility of contributions from electrets could not be eliminated.

In the present work, lithium disilicate crystals were crystallized from glasses which had the composition of 33.3 mole % Li_2O and 66.6 mole % SiO_2.

1.1 The System Li_2O-SiO_2

The system Li_2O-SiO_2 was selected for study for a number of reasons. The crystallization behavior of these glasses is well known and has been thoroughly reported[6].

Of the crystalline products in the glass-forming region, lithium disilicate was selected for study. Liebau reports the structure of lithium disilicate to be monoclinic in space group Cc and to have a strong orthorhombic pseudosymmetry. Unit cell dimensions with respect to the orthorhombic unit cell are a = 5.82Å, b = 14.66Å, and c = 4.79Å. Liebau determined that the structure consists of corrugated Si_2O_5 layers held together by lithium ions. Projections of the tetrahedra onto the three orthogonal planes appear in Figure 1. The orthorhombic c-axis is the polar axis. A projection of the crystal structure onto the (100) plane is presented in Figure 2. These diagrams clearly show the acentric, polar nature of the structure along the c-axis.

Single crystals of lithium disilicate would be expected to be both pyroelectric and piezoelectric in the c-direction. Attempts at growing single crystals have been made. These efforts result in bundles of needle-like crystals oriented with the c-axis parallel to the long direction of the crystallites. Optical examination shows that the crystallites are twinned on a very fine scale. Neither of the two possible polar directions of the c-axis is favored[8]. Because of the compensating effects of this extensive twinning, little or no pyroelectricity or piezoelectricity can be detected.

Crystals of lithium disilicate grown in glasses in the Li_2O-SiO_2 system have been shown to be highly oriented in thin layers near the surface of the glass[9,10]. These workers reported that the crystals in a thin layer near the surface have their c-axes perpendicular to the sample surface. The intention of the present work was to take advantage of this orientation phenomenon to produce a glass-ceramic in which the polar c-axis is aligned perpendicular to the sample surface. The mechanical interaction between the glass matrix and the crystallites might enhance the pyroelectric properties through the secondary effect.

2. Experimental

2.1 Sample Preparation

Reagent-grade acid and lithium carbonate were mixed in the proportions necessary to form glasses of composition $Li_2O{:}2SiO_2$. The mixture was melted in a platinum crucible in an electric furnace at temperatures in the range from 1400 to 1450°C for at least 24 hours. The fined glass was poured into graphite molds. The large residual stress from the rapid cooling was partially relieved by annealing for 12 hours at 400°C. Glass disks of varying thicknesses were produced by grinding and polishing the glass cylinders. Sample thicknesses ranged from approximately 130 micrometers to 5 millimeters.

Two general types of crystallization treatments were used. The treatment in which the entire sample was uniformly heated to the crystallization temperature will be termed "isothermal." Crystallization in which a thermal gradient is maintained in the samples will be termed "gradient crystallization. The isothermally crystallized samples were crystallized in a small electric tube furnace. The samples were quickly heated to 600°C and held at that temperature for one hour. All samples were cooled to room temperature from the crystallization temperature at a rate of approximately 100°C/minute.

The thermal gradient samples were prepared by polishing one end of a glass cylinder. The polished surface was placed on the heating element of a microscope hot stage. A small piece of platinum foil was placed between the heating element and the glass sample. The hot stage was heated to 600°C within 5 minutes to establish a thermal gradient across the sample. The temperature of the stage was increased to 800°C at the rate of 200°C/hour. The thermal gradient was estimated to be approximately 300°C/cm.

After cooling, the thermal gradient samples were thinned by grinding and polishing the cold end of the cylinders. X-ray and Chynoweth measurements were performed on the thin crystallized layer at the hot face of these samples.

At least one sample from each batch of glass was isothermally crystallized at 600°C and was ground to a powder. X-ray diffraction analyses were performed on a Picker diffractometer using CuK_α radiation. The patterns obtained were compared to standard patterns for phase identification.

To determine the degree of crystallite orientation in the samples, x-ray diffraction was performed on the as-crystallized surfaces. The relative peak heights from the crystallized samples were compared to the relative peak heights of the standard powder pattern to qualitatively evaluate the degree of orientation.

2.2 Pyroelectric Measurements

The pyroelectric responses were determined at room temperature using a method described by Chynoweth[11]. Sputtered gold electrodes were applied to both sides of the sample. Fine gold wires were attached to the electrodes using an air-drying silver paste. Radiation from a light source is chopped at a set frequency. The voltage developed across the sample is amplified and measured by a phase-sensitive detector. All measurements were compared with the signal from a sample of single crystals of lithium tantalate and tourmaline. The lithium tantalate standard also provided a means to standardize the various equipment parameters to obtain reproducible results.

The circuit shown in Figure 2 was employed to view the wave form generated by the samples. The signal from the FET amplifier was filtered to remove the 60 Hz and high frequency noise and the filtered signal was displayed on the oscilloscope. For the 5 Hz wave forms, the signal was first processed through a notch filter to remove the 60 Hz component. The signal was then processed through a bandpass filter to remove the high and low frequency noise. For the 0.5 Hz signal the 60 Hz noise was amplified, inverted, and added to the original signal to cancel out the noise by destructive interference. Photographs were taken of the image of the wave forms as displayed by a storage oscilloscope.

3. RESULTS AND DISCUSSION

The powder x-ray diffraction powder patterns for these glass-ceramics indicated that the only crystalline phase present in detectable quantities was lithium disilicate. No attempt was made to determine the stoichiometry of these samples from the x-ray patterns.

3.1 ISOTHERMAL CRYSTALLIZATION

Soaking times at the crystallization temperature were varied from one hour or more down to ten minutes. The samples crystallized for longer times, regardless of the presence or absence of an applied field, were completely opaque.

Those samples crystallized for shorter times were either translucent or slightly opalescent in appearance. In these samples, no bulk spherulitic crystallite growth could be observed with the unaided eye. These observations correspond to those made using the microscope hot stage. Surface crystallization occurs relatively quickly, but the nucleation and growth of the spherulites is a slower process. The short crystallization times result in surface crystallization but little or no visible crystallization of the bulk of the samples.

3.1.1 X-Ray Diffraction

In general, the x-ray diffraction patterns of the isothermally crystallized glass-ceramics showed that the sample surfaces contained highly oriented crystallites. As in the work of Rindone, the strong (002) reflection indicates that the crystallographic c-axis is perpendicular to the sample surface[9]. The degree of orientation was estimated by calcualting the ratio of the peak heights of the (002) to the (040) reflections. For random polycrystalline or powdered samples, this ratio is about 1:7. A higher ratio than this would indicate that the c-axis is preferentially aligned perpendicular to the sample surface. For the isothermally crystallized samples, this ratio was typically 100:1. Ratios as high as 300:1 were measured. Because of the high degree of orientation in many of these samples, it was often impossible to resolve the (130), (040), and (111) peaks. In these cases, this ratio was calculated on the basis of the height of the next highest peak in the range from 23 to 25 degrees 2-theta.

The ratios obtained from the diffraction patterns agree well with those obtained by Rindone for $Li_2Si_2O_5$ crystals in $Li_2O{:}4SiO_2$ glass[9]. He reported ratios as high as 500:1 for glasses crystallized without the addition of platinum nuclei.

The degree of orientation was dependent only on the quality of the surface finish. A sample which had been ground but not polished yielded an x-ray pattern very similar to that of a powdered sample. No enhancement of the 002:040 peak height ratio occurred unless the sample surfaces were highly polished prior to crystallization.

3.1.2 Microstructure

Microscopic examination of all of the samples was made. Etching the samples revealed the oriented surface crystallization detected by the diffractometer. Figure 4 is an optical photomicrograph of a typical layer. Figures 5-a and 5-b are SEM photomicrographs which show the needle-like lithium

disilicate crystals in these samples. The depth of the oriented layer in the isothermally crystallized samples varied from as little as 20 μm up to 250 μm. The depth of this layer was related to the length of time at the crystallization temperature. Those samples crystallized for short periods of time generally had thinner oriented layers. The bulk crystallization is spherulitic (and thus not oriented) in nature. The surface crystallization will grow into the sample until it encounters these spherulites. In the thicker samples the combination of oriented surface crystallization and the bulk spherulitic crystallization resulted in a sandwich structure. Figures 6-a and 6-b are optical photomicrographs of an isothermally crystallized sample which was approximately 0.08 cm thick.

The thinner samples consisted of the two layers of oriented crystallites extending inward from the surfaces but with no intervening layer of spherulitic growth. Figure 7 is a photomicrograph of a 0.013 cm sample. The two layers have apparently grown inwards towards the centerline of the sample faster than the rate of formation of the spherulitic crystallites. The thickness of the oriented layers is approximately 60 to 90 μm in these samples.

3.2 Thermal Gradient Crystallization

Macroscopically, the thermal gradient samples appeared to be crystallized on the hot surface to a depth of about two millimeters. The bulk of the sample remained non-crystalline with the exception of a few spherulites in the center of the sample.

3.2.1 X-Ray Diffraction

X-ray diffraction was performed on the crystallized surface. Peak height ratios (002:040) as high as 200:1 were measured. The degree of orientation was once again determined to be a function of surface finish only.

3.2.2 Microstructure

The depth of the oriented layer was as much as 1 mm, or at least four times greater than the layers in any of the isothermally crystallized samples. Figures 8-a and 8-b are photomicrographs of a typical thermal gradient sample showing the oriented layer of crystallites.

This technique enabled the preparation of samples in which a single oriented layer of lithium disilicate crystals could be grown to a substantial thickness.

3.3 Pyroelectric Measurements

Table 1 contains the results of the pyroelectric measurements on several of these samples. The voltage recorded in Table 1 is the voltage after amplification. All measurements were made at a frequency of 5 Hz.

The lithium tantalate sample used to standardize the equipment had the largest signal. The signals generated in the lithium disilicate samples were much smaller. The inverse relationship between the sample thickness and the magnitude of the signal was exhibited by the isothermally crystallized glass-ceramics.

The thermal gradient sample produced the largest signal of the glass-ceramics. For the purposes of comparison, a sample of single crystal tourmaline was ground and polished to a thickness close to that of the thermal gradient sample. Under identical conditions, the thermal gradient sample produced a signal which was approximately a factor of four larger than that produced by the tourmaline crystal.

It might be argued that the voltage signal in these samples may be related to effects other than pyroelectricity. There is, however, substantial evidence that pyroelectricity, whether primary or secondary due to mechanical interaction with the piezoelectric properties, is responsible for the signal.

First, the AC Chynoweth method eliminates many of the DC effects that are often measured as a material is heated. Thermoelectricity can contribute to the DC current, but the voltage generated during the time the light is on would rise to an equilibrium value and would not decay with time. The thermoelectric voltage would not change sign on cooling. Photoconduction and the trapping of charge carriers may result in the decay of the signal with time, but the sample would not recover to its original condition during the dark cycle[11].

The frequency dependence of the pyroelectric voltage response has been described by Putley[12]. For a true pyroelectric material, the log of the voltage should be a linear function of the log of the chopping frequency provided that the chopping frequency is greater than $1/\tau$, where τ is the electrical time constant for the detector-amplifier circuit. This frequency dependence has been plotted in Figure 9 for both the lithium tantalate standard

Table 1. Pyroelectric responses of $Li_2Si_2O_5$ glass-ceramics, lithium tantalate, and tourmaline

Material	Sample Thickness	Crystallization	Amplified Voltage (mV)	V Sample V $LiTaO_3$	Sample Capacitance at 1K	Tan δ
$LiTaO_3$	130 μm	Single crystal	350	1.0	74 pf	.005
$Li_2Si_2O_5$	800 μm	Isothermal	0.1	2.9×10^{-4}	.2 pf	∿.007
$Li_2Si_2O_5$	100 μm	Isothermal	1.9	5.4×10^{-3}	1.6 pf	∿.007
$Li_2Si_2O_5$	470 μm	Thermal gradient	11	3.1×10^{-2}	.4 pf	∿.007
Tourmaline	450 μm	Single crystal	2.7	7.7×10^{-3}	.4 pf	∿.006

Note: Amplifier input capacitance = 1 pf
Gain = 100:1

and a glass-ceramic sample. Note the linearity of both functions in this frequency range. This indicates that the frequency dependence of the signal in the lithium disilicate glass-ceramics follows the predictions of the pyroelectric theory.

The wave forms of the samples of lithium disilicate and lithium tantalate at chopping frequencies of about 5 Hz and 0.5 Hz, respectively, appear in Figures 10 and 11. The lower trace in the two photographs is the voltage drop across the photoresistor. The voltage of both samples rises to a maximum when the light is turned on and begins to decay with time. The voltage reverses when the light is turned off and again decays towards the baseline.

Given the tendency of the lithium disilicate crystals to twin on a very fine scale, the existence of pyroelectricity in these glass-ceramics is unexpected. In order for pyroelectricity to be detected in the oriented layers, the polarities of the crystallites cannot be randomly arranged. There must be some mechanism operating during crystallization which favors one polar sense of the c-axis over the other.

One possible mechanism involves the migration of alkali ions to the surface during heating. The explanation of the orientation effect in the surface layers of these glasses is based on the observation that the surface of an alkali-containing glass is higher in alkali concentration than is the bulk[10]. In a glass containing lithium, silicon, and oxygen, a high lithium concentration at the surface, if uncompensated by negative surface charges, must create an electric field within the glass. The surface of the glass would be expected to be positive with respect to the bulk. If lithium ion migration occurs prior to nucleation and crystallization, the electric field due to ion migration may influence the polar orientation of the crystallites within the oriented layer.

An alternative explanation based on lithium ion migration would be that the high lithium ion concentration at the surface favors the nucleation and growth of one of the two possible orientations through some mechanism not involving the electric field created by the ion migration.

If the migration of lithium ions towards the sample surfaces is held responsible for the favoring of one sense of the c-axis polarity over the other, then it must be true that the polarity of the two layers of oriented crystallites in the isothermally crystallized samples must be opposite to each other.

The accuracy of this statement can be tested by examining the phase relations between the light pulses heating the sample and the resultant voltage. For a single crystal such as the lithium tantalate standard, the polarity of the electrodes is independent of which surface is exposed to the light pulses. If the sample is inverted with respect to the light source, the sign of the detected voltage will not reverse.

This experiment was performed on the lithium disilicate samples. The samples which consisted of two oriented layers of crystallites separated by a spherulitic region did appear to reverse the sign of the voltage when inverted with respect to the light source. It was determined that the surface of the sample which is facing the light source was always positive with respect to the opposite surface. The samples behaved as if they consisted of two pyroelectric single crystals joined together such that the polar sense of the crystals opposed each other. This measurement indicated that the polarities of the oriented layers were in agreement with the proposed mechanism.

A further check was performed on samples which consisted of only a single oriented layer. Measurements of these samples showed that they behaved like single crystals. One surface always became positive regardless of which surface was exposed to the light pulses.

From these measurements it was concluded that the polarity of the crystallites in the oriented layers was not random. Some mechanism, probably related to the migration of lithium ions, was responsible for the favoring of one polar orientation over the other. The signal detected by the Chynoweth apparatus originates in the oriented layers. In those samples which consisted of two oriented layers separated by a random, spherulitic region, only the layer facing the light source contributes to the signal. The voltage induced across this layer by the temperature change is capacitively coupled to the opposite surface.

This explanation accounts for the relative magnitude of the signals generated by the glass-ceramics. In the thicker, isothermally crystallized samples, the signal originates in the oriented surface layer closest to the light source. The intervening spherulitic layer does not contribute to the response. The thinner isothermally crystallized samples give larger signals because of the reduced mass (and thus larger temperature change) but only one

layer can contribute to the signal. If the temperature of the second layer changes, it will tend to oppose the signal of the first layer. There is no opposing oriented layer in the thermal gradient samples to reduce the magnitude of the signal. These samples produced larger signals than the two-layer isothermally crystallized glass-ceramics.

4. CONCLUSIONS

Glass-ceramics containing highly oriented layers of $Li_2Si_2O_5$ crystallites have been made from glasses having the composition $Li_2O{:}2SiO_2$. The nucleation and crystallization behavior of this glass was found to be identical to the behavior of similar glasses as described in the literature. The highly oriented layers form at the surfaces of the samples prior to the nucleation and crystallization of spherulites in the interior of the samples. The degree of orientation was found to be dependent on the sample surface finish only.

Microscopic examination of the crystallized glasses showed that the oriented layers consisted of needle- or lath-like crystals oriented with their long axes perpendicular to the sample surface. The thickness of the oriented layers could be varied by varying the sample preparation and thermal treatment. Optimum layer thicknesses were obtained in samples which were crystallized by the application of a thermal gradient.

Pyroelectricity was detected in the crystallized glasses using the Chynoweth technique.

The existence of pyroelectricity in these glass-ceramics is evidence that there is a preferred orientation for the polar direction of the c-axes during crystallization of the oriented layer.

Although the absolute magnitude of the signals generated by these glass-ceramics is small compared to currently used pyroelectric detector materials, these samples represent the first reported non-ferroelectric pyroelectric glass-ceramics. The techniques and processes developed in this study may be applied to other systems to develop a new class of pyroelectric materials.

Acknowledgment

This work was sponsored by the Advanced Research Projects Agency (MDA 903-78-C-0306) and by the U.S. Army Research Office (DAAG29-80-C-0008.)

REFERENCES

1. A. Herzog, IEEE Trans. PHP-9, 247 (1973).
2. N.F. Borrelli, J. Appl. Phys. 38, 4243 (1967).
3. N.F. Borrelli and M.M. Layton, IEEE Trans. ED-16, 511 (1969).
4. M.M. Layton and J.W. Smith, J. Amer. Ceram. Soc. 58, 435 (1975).
5. A.M. Glass et al., Appl. Phys. Lett. 31, 4 (1977).
6. F.C. Kracek, J. Phys. Chem. 34,2641 (1930).
7. V.F. Liebau, Acta Cryst. 14, 389 (1961).
8. A. Bhalla, Private communication (1979).
9. G.E. Rindone, Symposium on Nucleation and Crystallization in Glasses and Melts, The American Ceramic Society, Columbus, Ohio, 19o2.
10. C.L. Booth and G.E. Rindone, J. Amer. Ceram. Soc. 47, 25 (1964).
11. A.G. Chynoweth, J. Appl. Phys. 27, 78 (1956).
12. E.H. Putley, Semicond. Semimetals, Volume 5 (Academic Press, NY 1970) p. 259.

LIST OF FIGURES

Figure 1. Arrangement of $(SiO_4)^{-4}$ tetrahedra in $Li_2Si_2O_5$.

Figure 2. Projection of the structure of $Li_2Si_2O_5$ onto the (100) plane.

Figure 3. Schematic of Chynoweth apparatus for wave form display.

Figure 4. Optical photomicrograph of surface crystallization (500X).

Figure 5. SEM photomicrograph of oriented, crystallized surface layer: (a) 700X; (b) 3000X.

Figure 6. Optical photomicrographs of isothermally crystallized glass-ceramic (100X).

Figure 7. Optical photomicrograph of isothermally crystallized glass-ceramic (200X).

Figure 8. Optical photomicrographs of oriented layer in thermal gradient sample (100X).

Figure 9. Pyroelectric response vs frequency for lithium tantalate standard and lithium disilicate glass-ceramic.

Figure 10. Wave forms of Chynoweth responses at 5 Hz: (a) $Li_2Si_2O_5$ glass-ceramic; (b) $LiTaO_3$ single crystal.

Figure 11. Wave forms of Chynoweth responses at 0.5 Hz: (a) $Li_2Si_2O_5$ glass-ceramic; (b) $LiTaO_3$ single crystal.

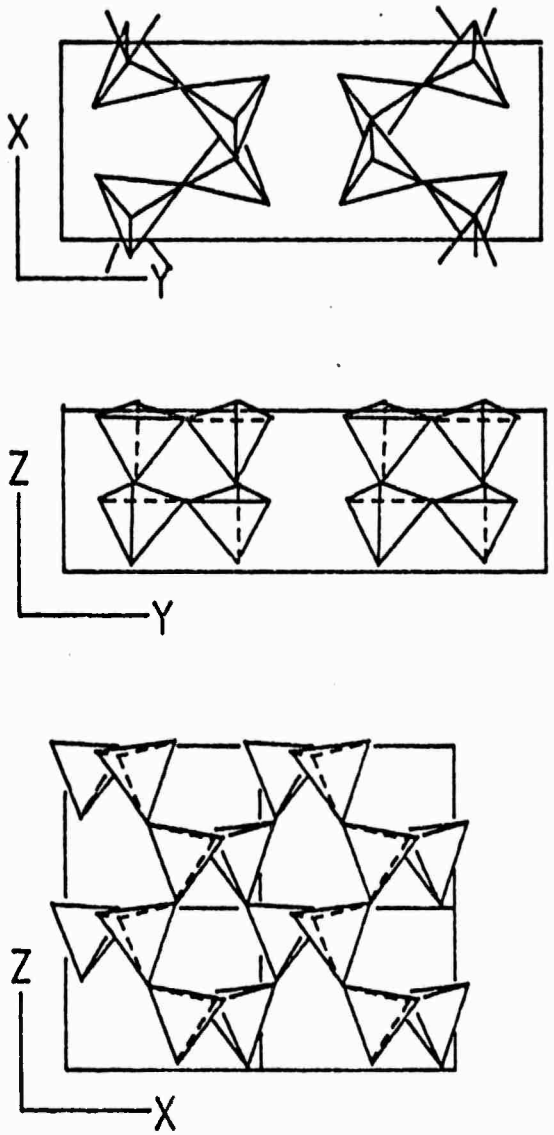

Figure 1 Arrangement of $(SiO_4)^{-4}$ Tetrahedra in $Li_2Si_2O_5$.

G. J. Gardopee, R. E. Newnham, A. S. Bhalla

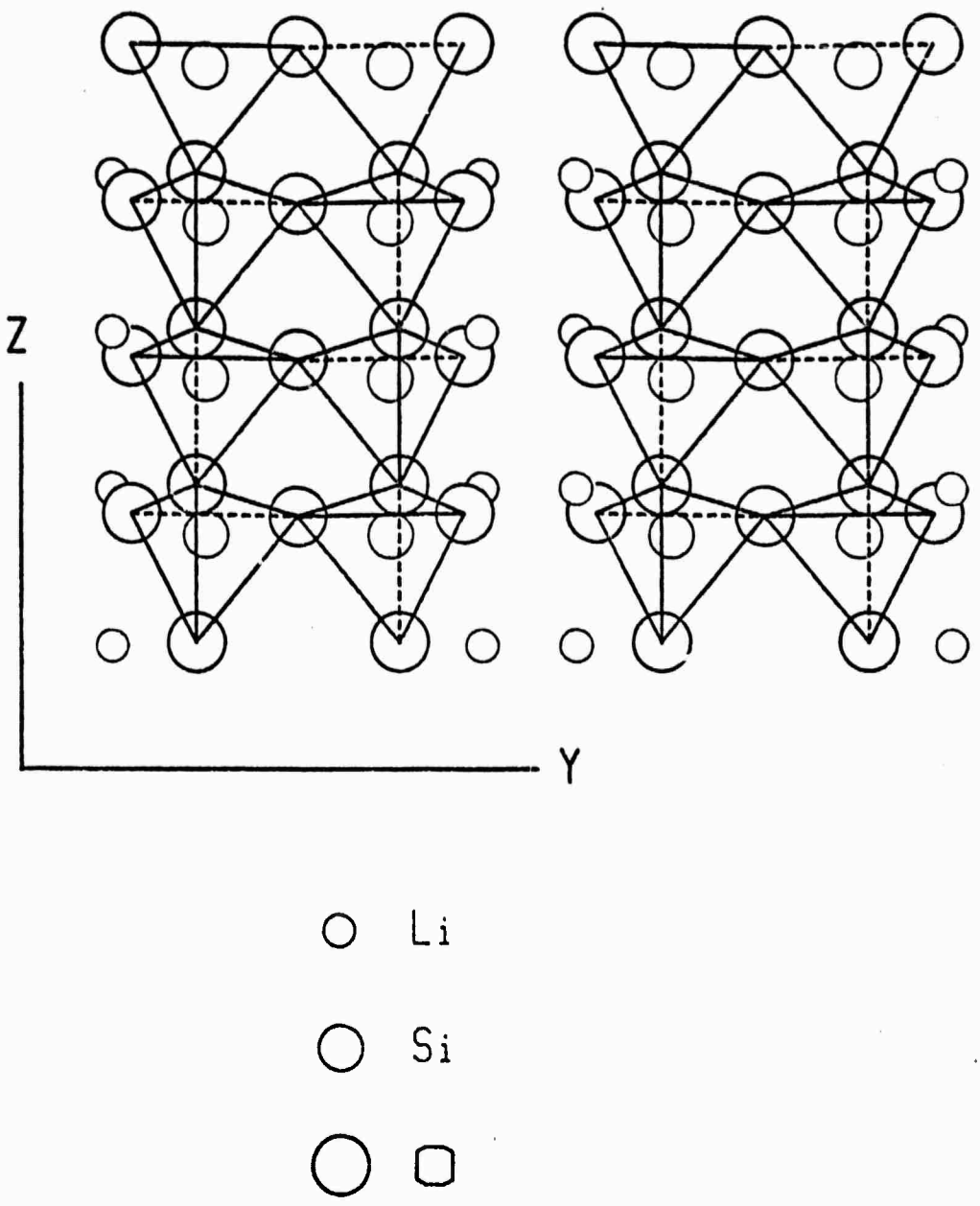

Figure 2. Projection of the Structure of $Li_2Si_2O_5$ onto the (100) Plane.

G.J. Gardopee, R.E. Newnham, A.S. Bhalla

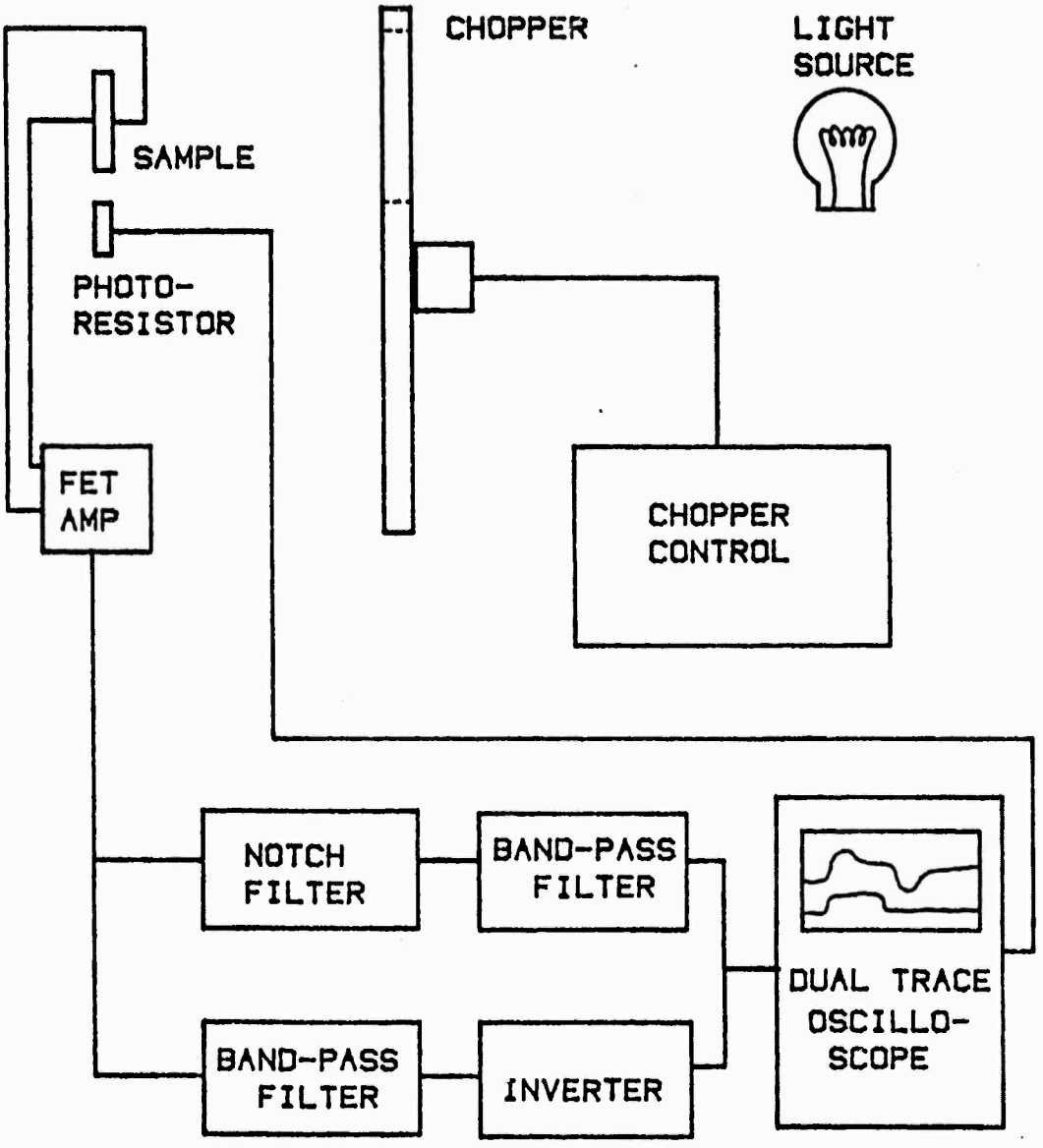

Figure 3. Schematic of Chynoweth Apparatus for Wave Form Display.

G.J. Gardopee, R.E. Newnham, A.S. Bhalla

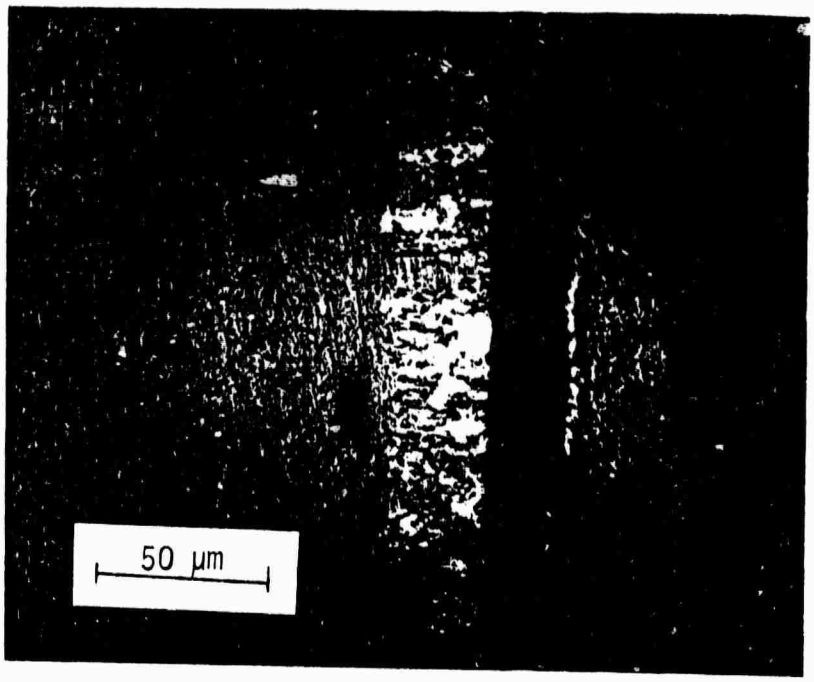

Figure 4 . Optical Photomicrograph of Surface Crystallization (500X).

G.J. Gardopee, R.E. Newnham, A.S. Bhalla

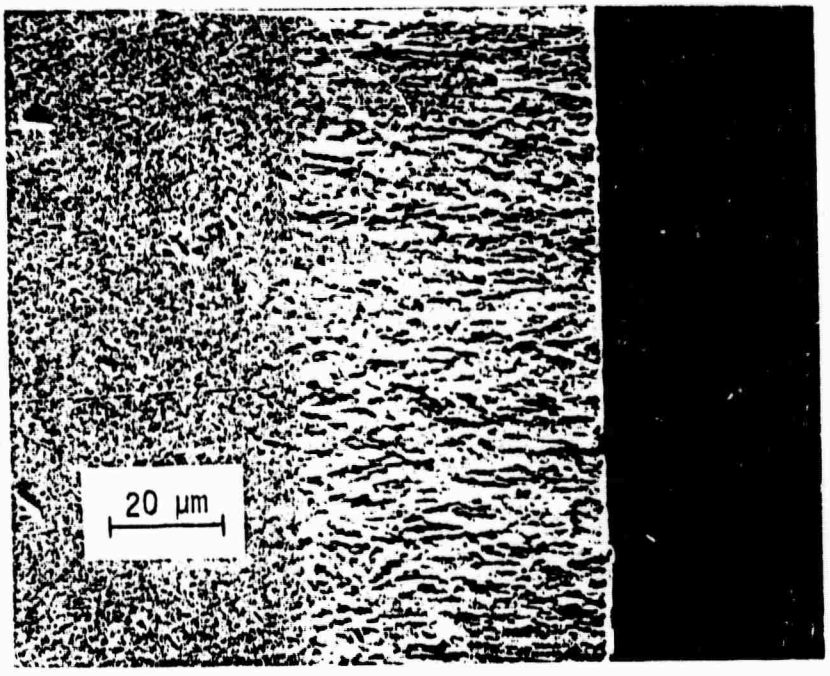

Non-Crystalline Bulk

Surface Layer

(a)

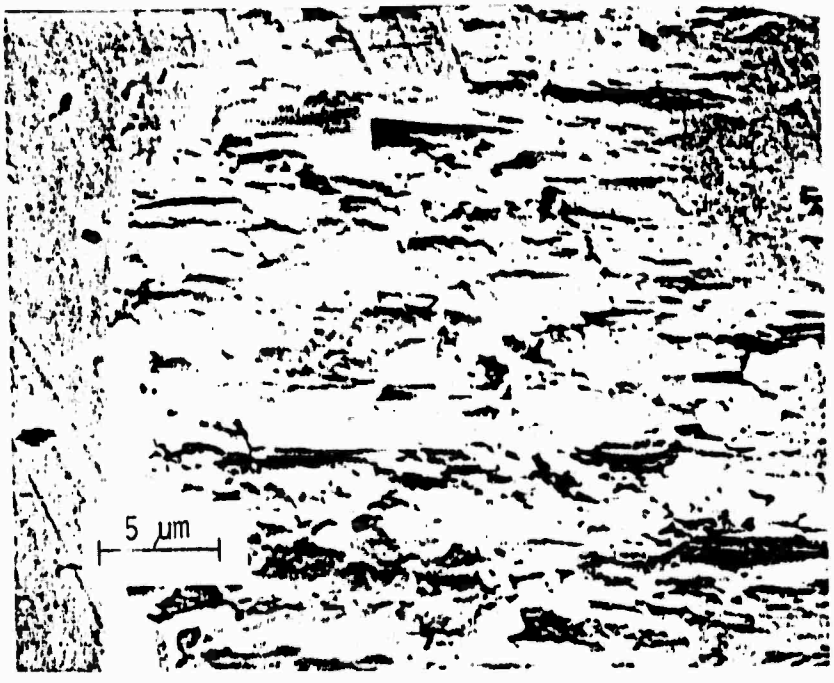

(b)

Figure 5. SEM Photomicrographs of Oriented, Crystallized Surface Layer: (a) 700X; (b) 3000X.

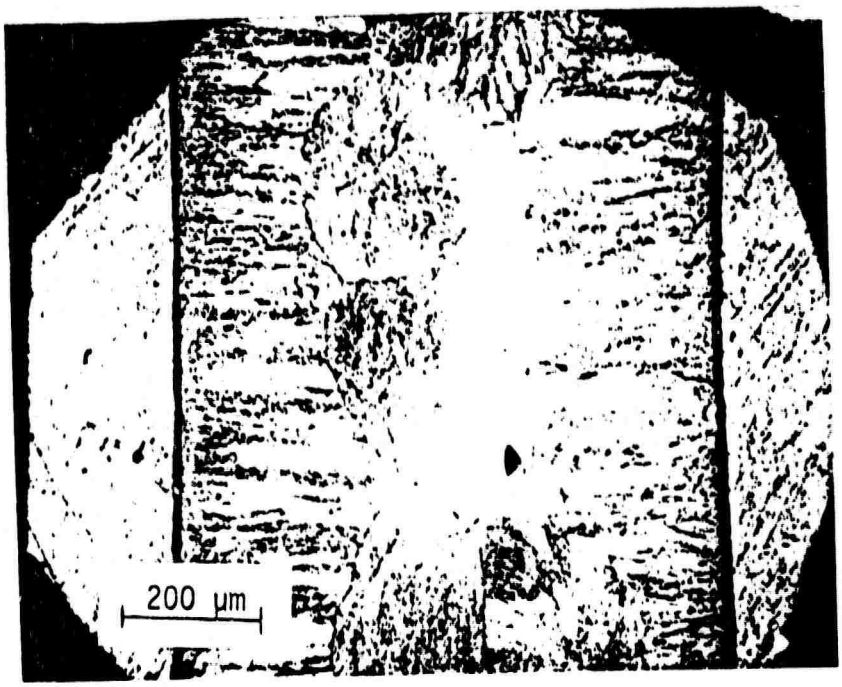

(a)

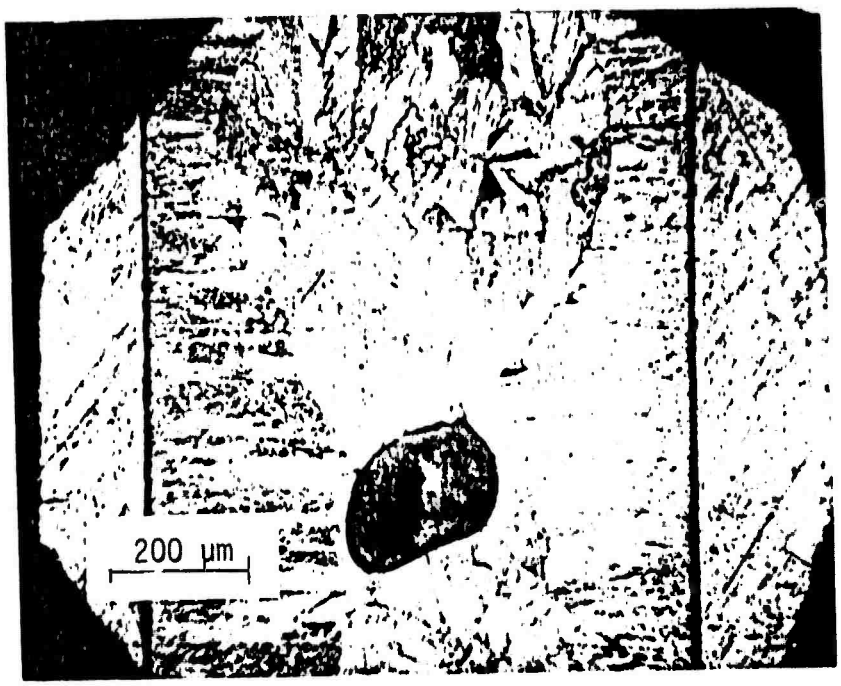

(b)

Figure 6 . Optical Photomicrographs of Isothermally Crystallized Glass-Ceramic (100X).

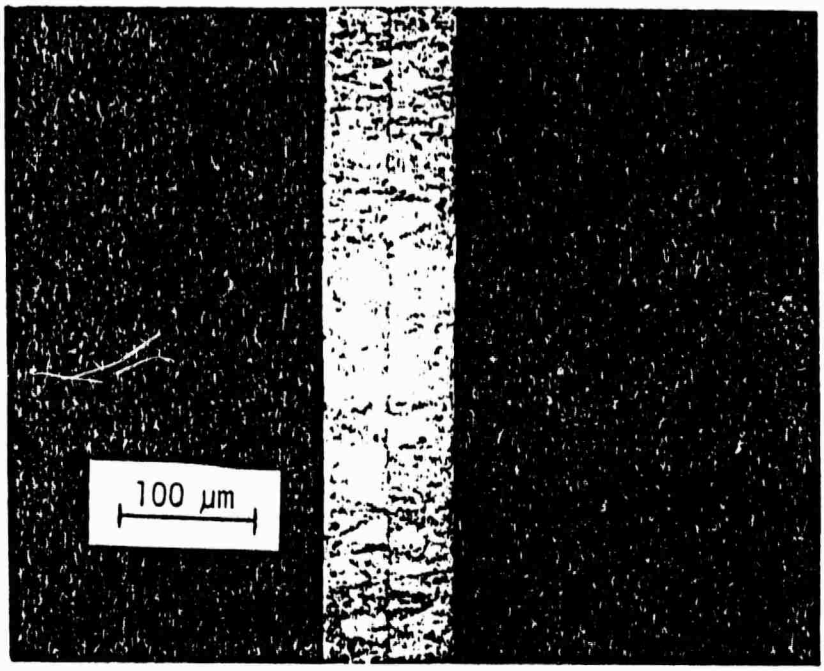

Figure 7. Optical Photomicrograph of Isothermally Crystallized Glass-Ceramic (200X).

G.J. Gardopee, R.E. Nehnham, A.S. Bhalla

(a)

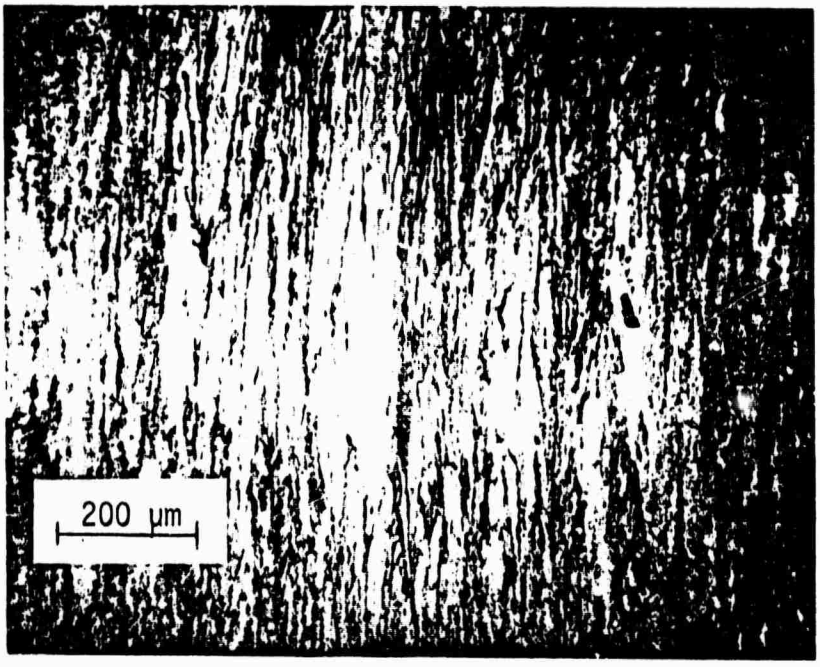

(b)

Figure 8. Optical Photomicrographs of Oriented Layer in Thermal Gradient Sample (100X).

G.J. Gardopee, R.E. Newnham, A.S. Bhalla

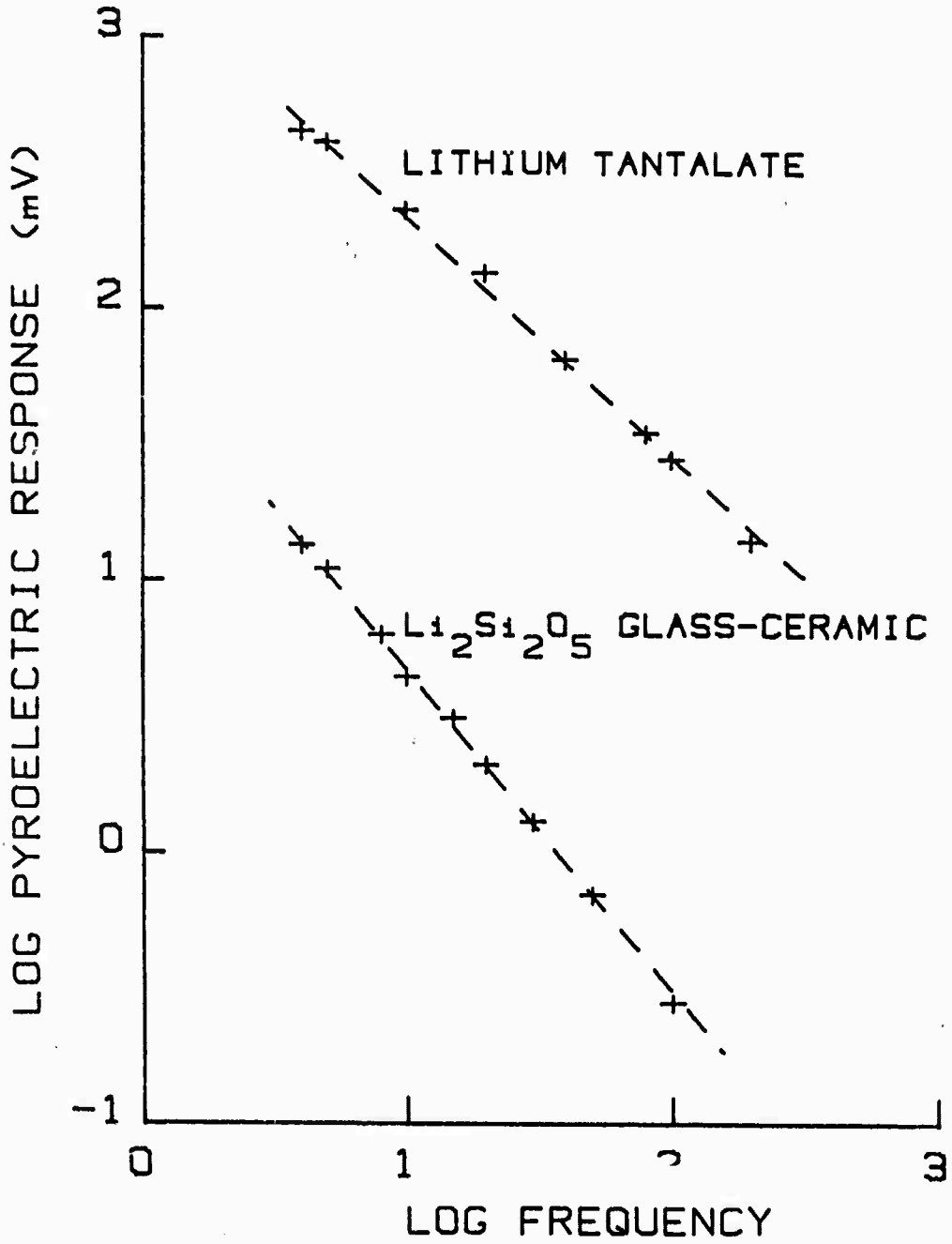

Figure 9. Pyroelectric Response vs. Frequency for Lithium Tantala Standard and Lithium Disilicate Glass-Ceramic.

G.J.Gardopee, R.E. Newnham, A.S Bhalla

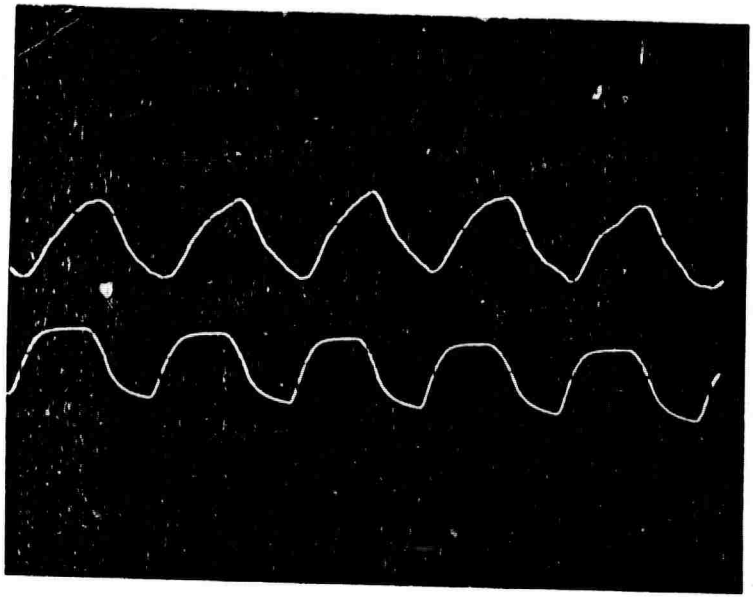

(a)

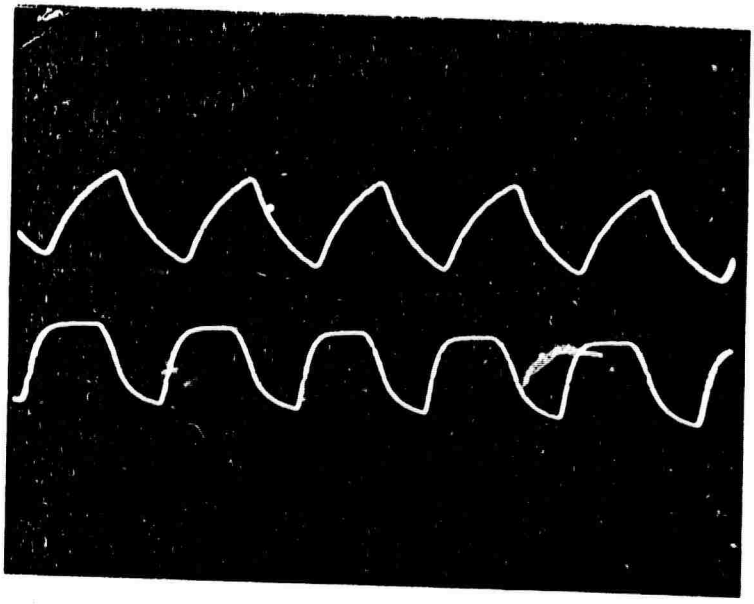

(b)

Figure 10. Wave Forms of Chynoweth Response at 5 Hz: (a) $Li_2Si_2O_5$ Glass-Ceramic; (b) $LiTaO_3$ Single Crystal.

G.J. Gardopee, R.E. Newnham, A.S. Bhalla

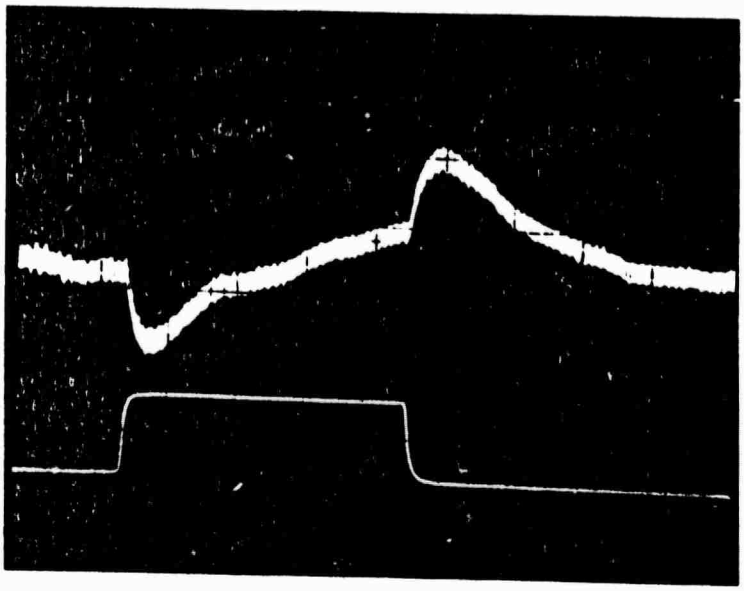

(a)

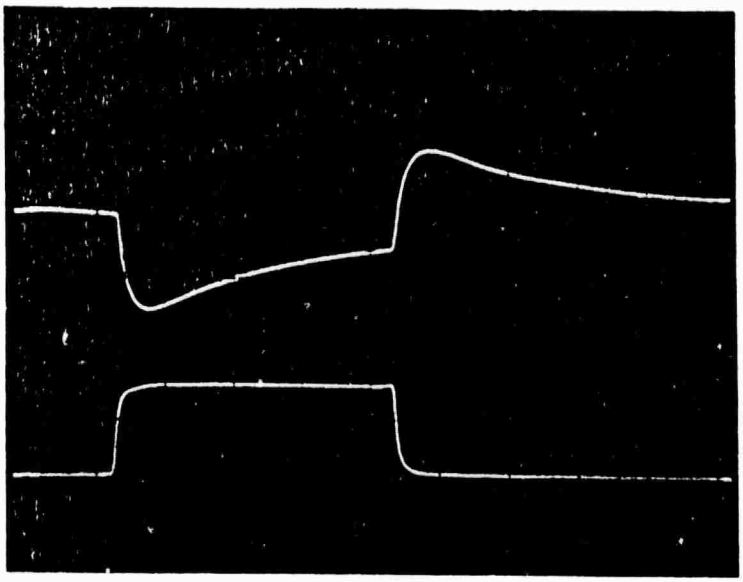

(b)

Figure 11. Wave Forms of Chynoweth Response at 0.5 Hz: (a) $Li_2Si_2O_5$ Glass-Ceramic; (b) $LiTaO_3$ Single Crystal.

G.J. Gardopee, R.E. Newnham, A.S. Bhalla

APPENDIX III

$Ba_2TiGe_2O_8$ and Ba_2O_8 Pyroelectric Glass-Ceramics

A. Halliyal, A. S. Bhalla, R. E. Newnham, L. E. Cross

$Ba_2TiGe_2O_8$ and Ba_2O_8 pyroelectric glass-ceramics

A. HALLIYAL, A. S. BHALLA, R. E. NEWNHAM, L. E. CROSS
Materials Research Laboratory, The Pennsylvania State University, University Park, Pennsylvania 16802, USA

Pyroelectric glass-ceramics of composition $Ba_2TiGe_2O_8$ and $Ba_2TiSi_2O_8$ were prepred by crystallizing the glasses in a temperature gradient. High pyroelectric responses up to 50% of the single-crystal values were observed because of the high degree of orientation of the crystallites in the glass-ceramic samples. The piezoelectric and dielectric properties of the glasses and the glass-ceramics are also consistent with the properties of the single crystals.

1. Introduction

Pyroelectric lithium disilicate glass-ceramics have recently been prepared by growing highly orientated surface layers of lithium disilicate crystals by crystallizing the glasses of stoichiometric glass compositions $Li_2O \cdot 2SiO_2$ in a temperature gradient [1]. The technique provides a method of fabricating large and inexpensive pyroelectric devices. However, one difficulty encountered in working with the lithium disilicate pyroelectric glass-ceramic was that thin targets (of thickness, $d < 200\,\mu m$) cut perpendicular to the growth direction (the polar c-axis of $Li_2Si_2O_5$) were extremely fragile and could not be prepared routinely.

In this study pyroelectric glass-ceramics of barium titatnium silicate (BTS: $Ba_2TiSi_2O_8$ or fresnoite) and barium titanium germanate (BTG: $Ba_2TiGe_2O_8$) are described, the physical properties of which are superior to $Li_2Si_2O_5$. Thin sections of these glass-ceramics, less than $100\,\mu m$ in thickness, can easily be prepared since they are mechanically much stronger. Glass-ceramics of BTG and BTS were prepared by crystallizing glasses of stoichiometric compositions of BTG and a silica-rich composition ($64SiO_2$–$36BaTiO_3$) of BTS in a thermal gradient. The dielectric and pyroelectric properties were measured and compared with the properties of single crystals.

In the single-crystal form fresnoite belongs to the crystallographic point group 4mm and is pyroelectric [2]. $Ba_2TiGe_2O_8$ is reported to be a ferroelastic [3, 4] below 810° C and belongs to the orthorhombic polar point group mm2. In the paraelastic phase above the transition temperature, T_c, BTG also belongs to the tetragonal point group 4mm.

Glass-ceramics in the $BaTiO_3$–SiO_2 system have been previously investigated. Herczog [5] studied the crystallization of $BaTiO_3$ in a silicate glass matrix. Dielectric and electro-optic measurements on transparent glass-ceramics containing ferroelectric $BaTiO_3$ in a glass matrix have also been reported [6]. However, the primary interest in these materials has been concerned with the dielectric and electro-optic properties of the glass-ceramics, and in the ferroelectric nature of $BaTiO_3$ crystallites surrounded by a glass matrix. In these studies no efforts have been made to develop glass-ceramics containing orientated crystallites. The present study describes the preparation and characterization of glass-ceramics containing orientated crystallites of the pyroelectric (but non-ferroelectric) BTS and BTG phases.

2. Experimental details

Glasses of composition $64SiO_2 \cdot 36BaO \cdot 36TiO_2$ were prepared by mixing reagent-grade silicic acid*, barium carbonate† and titanic oxide‡, followed by melting in a globar furnace. Fresnoite has a high melting point (1400° C) and thus, it was difficult to obtain bubble-free glasses of the stoichiometric composition. To avoid this problem, a composition was selected which lies near the eutectic point on the silica-rich side of the $BaTiO_3$–SiO_2 binary phase diagram [7]. This composition lies well within the range of glass formation in the $BaTiO_3$–SiO_2 system.

In the case of BTG, reagent-grade barium carbonate, germanium oxide‡ and titanic oxide were mixed and melted in the furnace. In both cases, the melts were maintained at 1375° C for 24 hours for fining and homogenization. Transparent samples were obtained by pouring the melt into a graphite mould. The samples which crystallized during pouring of the melt were remelted

and poured again into the graphite mould in order to ensure transparent glass samples. All the glass samples were annealed at 600° C for 12 hours and then cut and polished in the form of thick disks in preparation for the crystallization studies. To determine the crystallization temperatures of the glass compositions, differential thermal analysis (DTA) measurements were performed on the glass samples. Exothermic peaks were observed at 860° C in the case of BTS and at 800° C in the case of BTG, as shown in Fig. 1.

Crystalization was carried out in a temperature gradient by placing the polished glass samples, in the form of thick disks, on a microscope hot stage.§ The temperature gradient near the hottest temperature zone was perpendicular to the surface of the sample and it was estimated to be about 100° C mm^{-1}. Typical heating cycles used for glass crystallization are shown in Fig. 2. The heating cycle consisted of an initial rapid rise in temperature to minimize volume nucleation, followed by a slow increase in temperature at a rate of about 3° C min^{-1}. After reaching the maximum crystallization temperature (1100° C for BTS and 1000° C for BTG), the samples were held at this temperature for 24 hours. The temperature was then decreased rapidly to room temperature. The thicknesses of the crystallized portions of the glasses ranged from 1 to 2 mm, depending on the heating cycle.

The degree of preferred orientation of the glass-ceramic was evaluated from X-ray diffractometer patterns. X-ray diffraction (XRD) patterns were recorded on surfaces normal to the direction of the temperature gradient (Fig. 4). The XRD patterns were compared with the standard powder diffraction patterns to determine the relative degree of orientation. The dielectric constants of glass and glass-ceramic disks were measured with a capacitance bridge. The piezoelectric behaviour parallel to the crystallization direction was studied using a d_{33}-meter*. The samples were thinned down to about 200 μm in thickness and the pyroelectric response was measured by the dynamic Chynoweth technique [8] at a modulating frequency of 41 Hz. The pyroelectric signals on glass-ceramics were compared with the responses from single crystals of the BTG and BTS. The densities of BTG, BTS glasses and glass-ceramic samples were determined by a mercury porosimeter† and compared with the densities of single crystals.

3. Results and discussion

Table I summarizes the data for the glass and glass-ceramic samples. Single-crystal values are also listed for comparison.

X-ray powder diffraction patterns of the crystallized samples showed that the principal crystallized phases were fresnoite in the BTS glass-ceramics and $Ba_2Ge_2TiO_8$ in the BTG glass-ceramic samples. A few low-intensity peaks of an unidentified phase were observed in the powder diffraction patterns of both compositions. The samples showed highly orientated crystal growth in a direction parallel to the temperature gradient, with the polar *c* axis perpendicular to the hot surface of the sample. As shown in Fig. 3, the 002 reflection was the strongest in the X-ray patterns of the crystallized surfaces. The ratio of the intensity of the 002 peak to that of the 211 peak was taken as a measure of the relative degree of orientation. The intensity ratios are given in Table I. Comparison of the intensity ratios in the glass-ceramic samples with the intensity ratios of a standard powder pattern, showed a high degree of orientation of the crystallites in the glass-ceramics. An even higher degree of orientation was obtained in the samples with good surface finish.

The degree of preferred orientation in crystallized samples of BTS and BTG was similar to that observed previously [1] in $Li_2Si_2O_5$. It was observed that the degree of orientation of the crystallites in the isothermally crystallized glass-ceramics was poor compared to the samples crystallized in a temperature gradient. In addition, detailed studies of the microstructure of the crystallized samples showed that the thickness of the well-orientated region was larger in the case of samples crystallized in a temperature gradient, indicating that thermal gradient crystallization is preferable for obtaining well orientated glass-ceramics.

The main reason for the orientation of the crystallites is surface-nucleated crystallization which takes place in both the isothermal and temperature-gradient crystallization. A higher degree of electrical and crystallographic orientation is obtained in the temperature-gradient crystallization method due to the absence of volume nucleation; however, in the case of isothermal crystallization, the orientation of the crystallites is limited to a layer only a few micrometers thick due to the simultaneous occurrence of volume nucleation. Atkinson and McMillan [9] attempted to produce a $Li_2Si_2O_5$ glass-ceramic with an aligned microstructure by a hot extrusion method. They were partially successful in obtaining glass-ceramic samples with the disilicate crystal crystallographically-aligned parallel to the extrusion axis. However, the degree of orientation of the crystallites was less than that obtained in glass-ceramic samples prepared by crystallizing the glasses in a temperature gradient [1].

The density of BTG glass was about the same as the single-crystal form (Table I), while that of BTS glass was slightly lower than the density of fresnoite single crystals because of the excess silica used in the BTS composition. Only a small decrease in density occurred on crystallization of the glass phases, indicating a low concentration of voids in the glass-ceramic samples. Samples as thin as 100 μm could be prepared without difficulty because of the absence of pores and cracks.

The dielectric constants of BTS and BTG glasses measured at 1 MHz are very close to the mean dielectric constant, $(\epsilon_{11} + \epsilon_{22} + \epsilon_{33})/3$, of the corresponding crystalline phases. On crystallization, the dielectric constant of the glass-ceramic samples show a slight decrease; the dielectric constant measured in the crystallization direction is closer to the ϵ_3-values of the single crystals. This is consistent with the fact that the c-axis is the preferred orientation direction in the glass-ceramic, as indicated by X-ray diffraction analysis.

The loss tangent factors of the glass-ceramics were similar to those measured on single crystals.

Piezoelectric coefficients, d_{33}, measured in the crystallization direction in glass-ceramics were comparable to the single-crystal d_{33} coefficient values reported [2–4] for BTS and BTG. Opposite faces of the sample gave opposite signs for the piezoelectric constant. The large magnitude of d_{33}-values and its sign reversal suggest that the crystallites in the glass-ceramics are not only orientated along the c-axis in the crystallization direction, but that most of the crystallites have the same polarity as well. The fact that the d_{33}-values remained constant over the entire surface of the glass-ceramic testifies to the uniformity and the homogeneity of the samples.

As in the previous study of lithium disilicate [1], it was observed that the temperature gradient dictated both the electrical and crystallographic alignment. In all samples the polar orientation was antiparallel to the direction in which crystallization proceeds into the glass, with the positive end of the dipole pointing toward the high-temperature end of the sample, as depicted in Fig. 4. There may be several causes for the polar alignment of the crystallites. One possible cause is the existence of high local electric fields resulting from surface pyroelectric charges [10]. These local electric fields might dictate the orientation of the dipoles as crystallization proceeds into the glass. A second possible cause is the nature of the surface chemistry. It is known that low charge cations such as Li^+ or Ba^{2+} migrate to the surface upon heating [11]. This higher surface concentration of cations could influence the nature of both the crystallization and polar orientation. It is possible that as the crystallization proceeds into the bulk of the glass, starting from a cation-rich surface, the positive end of the dipole moments in the crystallites will be directed toward the hot surface.

The pyroelectric response on the glass ceramics was studied by the dynamic Chynoweth method. Pyroelectric voltage responses of between 50 and 60% of the single-crystal values were obtained reproducibly with the glass-ceramic samples. The sign of the pyroelectric coefficient is negative for BTG single crystals and positive for BTS. A similar difference in sign was observed with glass-ceramics. For a simple pyroelectric detector, the figure of merit is given by p/ϵ, where p is the pyroelectric coefficient and ϵ is the dielectric permittivity. The pyroelectric coefficients of single crystals of $Ba_2TiGe_2O_8$ and $Ba_2TiSi_2O_8$ are 3 and 10 $\mu C m^{-2\,\circ} C$, respectively [12]. Since the dielectric constants of the glass-ceramics are comparable with those of single crystals, it can be concluded that the pyroelectric coefficients of the glass-ceramics are of the same order of magnitude as the single crystals. Specimens of 100 to 500 μm in thickness were studied during pyroelectric tests. Samples of large surface area and less than 100 μm were mechanically strong and gave reproducible results, suggesting their use as pyroelectric detectors.

4. Conclusions

Glass-ceramics of composition $Ba_2TiGe_2O_8$ and $Ba_2TiSi_2O_8$ were prepared by crystallizing the glasses in a temperature gradient. The glass-ceramics show preferred orientation, with the polar c-axis parallel to the temperature gradient. Pyroelectric responses up to 50% of the single-crystal values were observed on these glass-ceramic samples. Measurement of the density, dielectric constant, and piezoelectric constant gave results comparable to the reported single-crystal properties.

Acknowledgement

We wish to thank our colleagues at the Materials Research Laboratory for their advice and assistance. This work was sponsored by the U.S. Army Office of Research and Development (Contract Grant No. DAAG29-78-0033) and by Defense Advanced Research Projects Agency (Contract DARPA Project No. P-15124-MS).

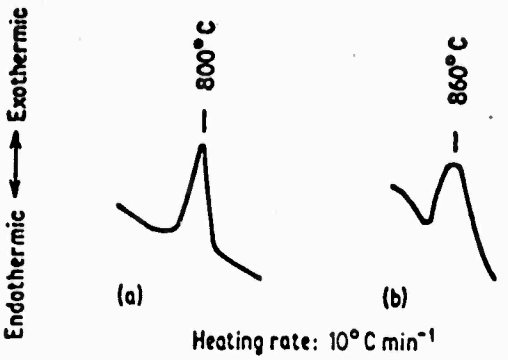

Figure 1 DTA heating curves of (a) BTG and (b) BTS glasses.

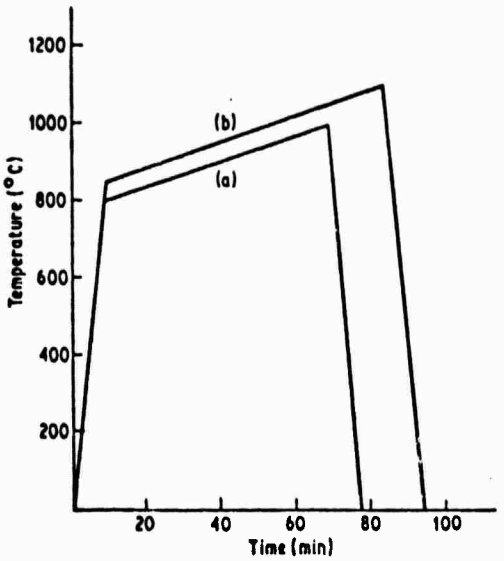

Figure 2 Heating cycles used for crystallizing (a) BTG and (b) BTS glasses.

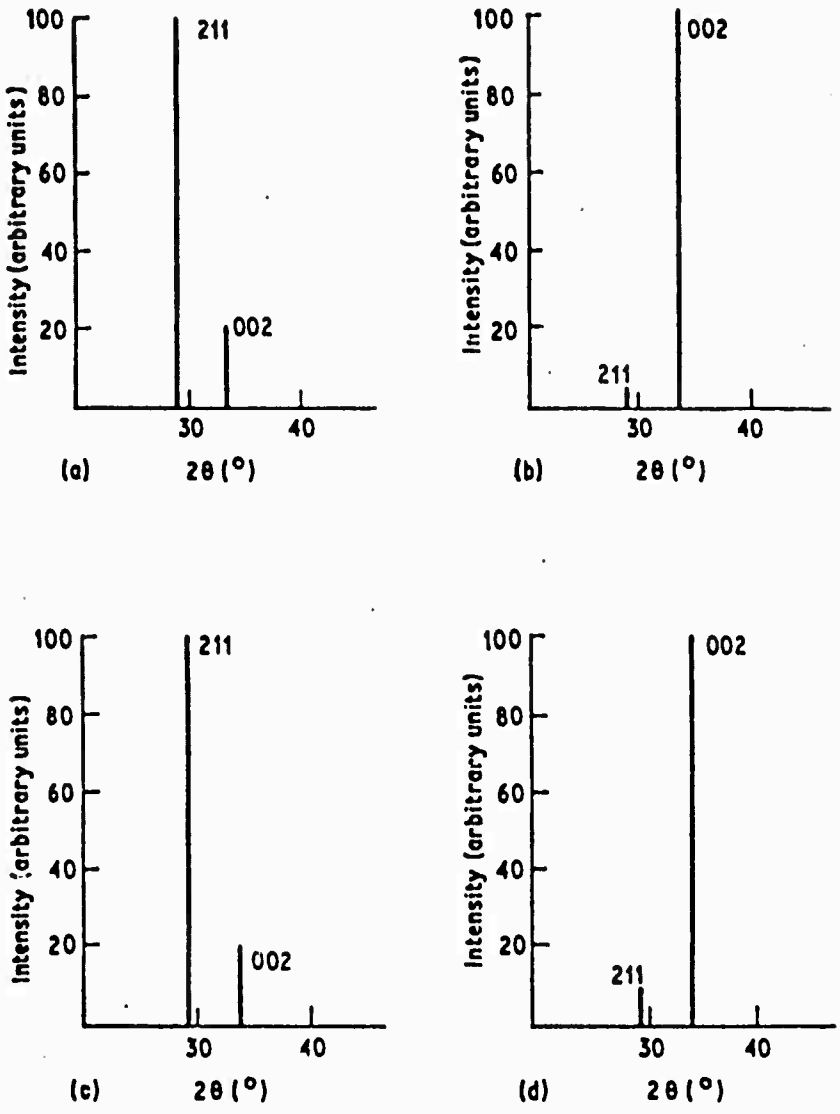

Figure 3 X-ray diffraction patterns of (a) $Ba_2Ge_2TiO_8$ standard powder diffraction pattern, (b) BTG glass-ceramic, (c) $Ba_2TiSi_2O_8$ standard powder diffraction pattern, and (d) BTS glass-ceramic.

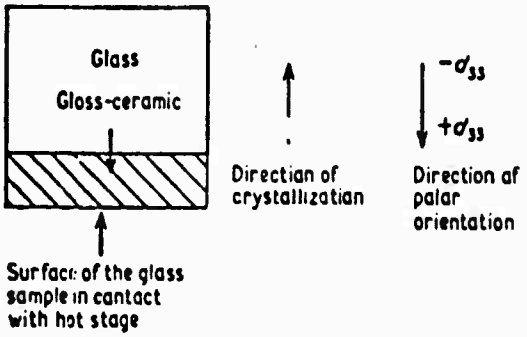

Figure 4 The direction of polar orientation in glass-ceramic samples.

References

1. G. J. GARDOPEE, R. E. NEWNHAM, A. G. HALLIYAL and A. S. BHALLA, *Appl. Phys. Lett.* 36 (1980) 817.
2. M. KIMURA, Y. FUGINO and T. KAWAMURA, *ibid.* 29 (1976) 227.
3. M. KIMURA, K. DOI, S. NANAMATSU and T. KAWAMURA, *ibid.* 23 (1973) 531.
4. M. KIMURA, K. UTSUMI and S. NANAMATSU, *ibid.* 47 (1976) 2249.
5. A. HERCZOG, *J. Amer. Ceram. Soc.* 47 (1964) 107.
6. N. F. BORRELLI and M. M. LAYTON, *J. Non-Cryst. Sol.* 6 (1971) 197.
7. D. E. RASE and R. ROY, *J. Amer. Ceram. Soc.* 38 (1955) 393.
8. A. G. CHYNOWETH, *J. Appl. Phys.* 27 (1956) 78.
9. D. I. H. ATKINSON and P. W. McMILLAN, *J. Mater. Sci.* 12 (1977) 443.
10. P. E. BLOOMFIELD, I. LEFKOWITZ and A. D. ARONOFF, *Phys. Rev. B* 4 (1971) 974.
11. G. E. RINDONE, in Proceedings of the Symposium on Nucleation and Crystallization in Glasses and Melts, edited by M. K. Roser, G. Smith and H. Insley (American Ceramic Society, Columbus, Ohio, 1962) pp. 63–69.
12. A. S. BHALLA, unpublished work.

*J. T. Baker Chemical Co., Phillipsburg, NJ, USA.

†Fisher Scientific Co., Phillipsburg, NJ, USA.

‡Eagle–Picher Industries, Inc., Quapaw, Oklahoma, USA.

§Model No. 493, manufactured by E. Leitz, Inc., Rockleigh, NJ, USA.

*Model CPDT 3300, manufactured by Channel Products, Chesterland, OH, USA.

*Model JS-7146, manufactured by American Instrument Co., Silver Spring, MD, USA.

APPENDIX IV

Paper Presented at the American Crystallographic Association Meeting, March 1980, Alabama

PYROELECTRIC GLASS-CERAMICS*. R. E. Newnham, G. J. Gardopee, A. Halliyal and A. S. Bhalla, Materials Research Laboratory, The Pennsylvania State University, University Park, Pennsylvania 16802.

Glass-ceramics containing highly oriented layers of $Li_2Si_2O_5$ crystallites have been made from glasses of identical composition. The nucleation and crystallization behavior of the glass resembles that of similar glasses described in the literature. Highly oriented layers form at the surface of the sample prior to the nucleation and crystallization of spherulites in the interior. The degree of orientation depends mainly on the surface finish. The crystal structure of $Li_2Si_2O_5$ belongs to point group mm2, with the polar axis parallel to the needle axis of the crystallites. Microscopic examination of the crystallized glasses showed that the oriented layers consisted of needle-like crystals oriented with the polar axis perpendicular to the sample surface. X-ray diffractometer patterns were used to estimate the degree of orientation. The thickness of the oriented layers could be controlled by varying the sample preparation and thermal treatment. Optimum layer thicknesses were obtained in samples crystallized under a thermal gradient. Pyroelectricity was detected in the crystallized glasses using the Chynoweth technique. The signals generated by glass-ceramics crystallized in a thermal gradient were approximately four times larger than that of a tourmaline crystal of similar dimensions. The time dependence of the pyroelectric responses were found to closely fit the thin-layer equivalent circuit model developed by Chynoweth. Although the absolute magnitude of the signals generated by the $Li_2Si_2O_5$ glass-ceramics is small compared to currently-used pyroelectric detector materials, these samples are the first example of a non-ferroelectric pyroelectric glass-ceramic. The process for making these new pyroelectric materials is amenable to mass production.

*This work was supported by the U.S. Army under Contract DAAG-29-76-G-0145, and by Defense Advanced Research Projects Agency, Contract MDA903-78-C-0306.

APPENDIX V

Pyroelectricity in SbSI

A. S. Bhalla, R. E. Newnham and L. E. Cross

PYROELECTRICITY IN SbSI

A. S. BHALLA, R. E. NEWNHAM and L. E. CROSS

Materials Research Laboratory, The Pennsylvania State University, University Park, Pennsylvania 16802

and

J. P. DOUGHERTY† and W. A. SMITH

North American Philips, Briarcliff Manor, NY 10510

(*Received July 30, 1980*)

Large pyroelectric coefficient (1.2×10^4 $\mu C/m^2 °C$ at $T - T_c \simeq 2°C$) in single crystals of SbSI were measured over a temperature range encompassing the ferroelectric phase transition. Simultaneous measurement of the pyroelectric and dielectric constants were made and the pyroelectric figure of merit p/K was evaluated at various temperatures.

INTRODUCTION

Antimony sulfur iodide (SbSI) is the most important member of a family[1,2] of ferroelectric semiconductors with formula $A^{V}B^{VI}X^{VII}$. It has a displacive first order ferroelectric transition near 20°C. The Curie temperature T_c depends on the growth method and chemical stoichiometry of the crystal.[3,4] In the ferroelectric phase, SbSI belongs to point group mm2 in the orthorhombic system and exhibits a very large structural anisotropy along the polar c-axis.[5,6] The transition is accompanied by an exceedingly high permittivity at T_c. Crystals grow as bundles of fine needles parallel to the c-axis making it rather difficult to obtain good electrical measurements on these crystals because of their small cross-sectional area and the uncertainty of the single-crystal nature of the sample. So far, no reliable measurements of the pyroelectric coefficient and its temperature dependence have been reported in the literature. In this paper we describe the simultaneous measurement of the pyroelectric and dielectric constants[7] on SbSI crystals using a modified Byer-Roundy method.[8] This technique eliminates uncertainties in temperature by measuring p and ϵ simultaneously. The pyroelectric figure of merit p/ϵ is evaluated over a temperature range encompassing the ferroelectric phase transition.

MEASUREMENT TECHNIQUE

Measurement of the pyroelectric coefficient p and the dielectric permittivity ϵ was carried out using an automated measurement technique.[7] In this system, the pyroelectric coefficient is determined by measuring the DC discharging (or charging) current (i) from a sample of known electrode area (A) subjected to a controlled rate of change of temperature (dT/dt). The pyroelectric coefficient p is given by

$$p = \frac{i/A}{dT/dt} \tag{1}$$

It is important to compare the measured pyroelectric coefficient for both heating and cooling over a number of temperature cycles because there are several possible sources of current arising from the release of trapped or injected charge and from conduction currents under bias. Comparing heating and cooling curves after different modes of poling and under different cycling conditions provides a way of eliminating some of these extraneous effects.

† Present Address: Gulton Industries, 212 Durham Avenue, Metuchen, NJ 08840.

Simultaneous pyroelectric and dielectric measurements are made by dividing the circuit into high and low frequency parts. The low frequency (essentially DC) side of the circuit is used to apply the DC bias and measure the capacitance at 1 MHz through the high frequency branch of the circuit. The two halves are electrically isolated from each other. Automated control is accomplished with a Hewlett-Packard 3052A Automated Data Acquisition System. The pyroelectric measurement system is based on a HP9825A minicomputer with instrument control and data transfer provided by the HPIB interface bus (IEEE 488 Standard). Data are stored on magnetic tape cartridges and plotted on a digital plotter. The computer controls the temperature (heating rate) and bias applied to the sample. The overall system speed is 3 to 4 complete measurement cycles per second with data stored only when any one of the measured quantities exceeds a preset percentage of absolute change.

The sample temperature is determined with the well-calibrated platinum resistance thermometer. Time is determined using an HP98035A interface clock. From the time and temperature measurements, dT/dt is calculated. In our arrangement, the pyroelectric coefficient can be studied in the temperature range between −30 and 200°C.

EXPERIMENTAL

Crystals of SbSI were grown from an SbI_3 flux using the Bridgman method and a vapor transport technique.[9,10] A few good quality single crystals with well-defined morphology were selected. Crystals were examined with a polarizing microscope for optical quality and foreign inclusions. Chemical homogeneity was evaluated by electron microprobe analysis in a scanning electron microscope. Vapor-grown crystals were slightly off stoichiometry with a slight excess of sulfur together with oxygen impurities. Cross-sectional areas of the crystals were measured by optical microscopy. Two ends of the crystals were electroded with Ag-paste, and gold wires 5 mil in diameter were attached to the ends. Crystals were suspended from the gold wire electrodes in a special specimen holder and then positioned in a silicone oil bath. The SbSI samples were kept dark to avoid the possibility of photocurrents. Samples were poled with DC fields of 500 V/cm to 1 KV/cm while being cooled from 45°C to about 10°C. At 10°C the poling field was removed gradually in order to minimize the possibility of back switching caused by the space charge built up under DC field. Samples were held at that temperature up to several hours before collecting the pyroelectric data in the heating cycles. Typical heating rates were 1°C/min to 4°C/min in various runs.

RESULTS AND DISCUSSION

Figure 1 shows the temperature dependence of the dielectric constant of vapor-grown SbSI measured at MHz with and without extra bias. An electric field of −800 V/cm was applied while heating the crystal in Run No. 1 and during the cooling cycle in Run No. 2. In Run No. 3 the sample was heated at 2°C/min from 5°C to 40°C under zero field. Simultaneous measurements of the sample capacitance and the pyroelectric output current were made. The sample was then cooled through the phase transition under a positive field of 800 V/cm. Dielectric and pyroelectric data were again collected in Run No. 5 while heating the sample.

Figure 2 shows the current density measured during cycles No. 3 and 5. The change in sign of the current density with the reversal of the poling field indicates clearly that the origin of the current is the pyroelectric effect in SbSI. The pyroelectric coefficients calculated from Eq. 1 are plotted in Figure 3 for various temperatures. The pyroelectric coefficients are unusually large, even at temperatures well removed from the transition (Figure 4). In the vapor-grown crystals, typical values of the pyroelectric coefficients were 1.2×10^4

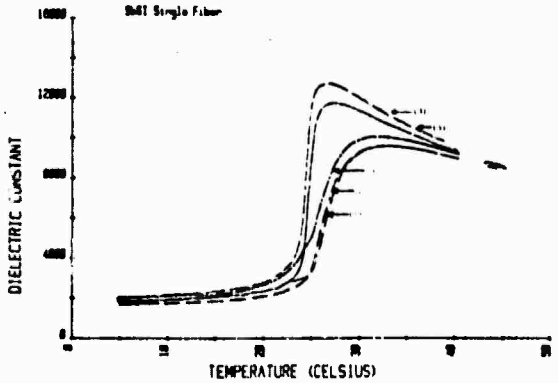

FIGURE 1 Temperature dependence of the dielectric constant of vapor grown SbSI at 1 MHz. (1) and (2) with bias-800 V/cm, (3) no bias, (4) bias + 800 V/cm, and (5) no bias.

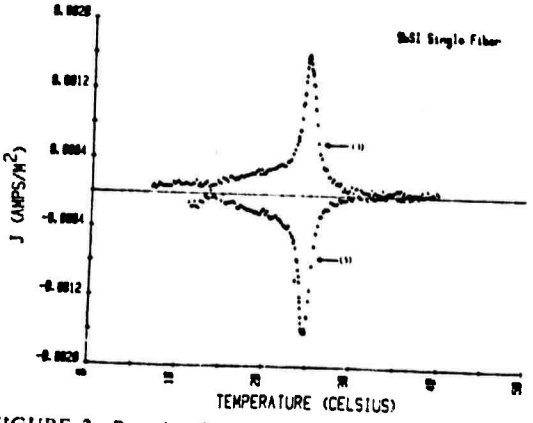

FIGURE 2 Pyroelectric current density with the reversal of the poling field.

$\mu c/m^2{}^\circ K$ at $(T-T_c) = 2°$ and 6×10^4 $\mu c/m^2{}^\circ K$ at the peak respectively. The spontaneous polarization (P_s) 23 $\mu c/cm^2$ (Figure 5) calculated from the integration of pyroelectric current agrees well with the value of 25 $\mu c/cm^2$ reported in the literature.

Both the dielectric and the pyroelectric data show a sharp transition around 24.7°C, slightly higher than the value reported for flux-grown crystals. Apparently the vapor-grown crystals contain oxygen impurities and excess sulfur which result in a small increase in the transition temperature. The pyroelectric properties are relatively unaffected by the small amount of impurities, as evident from the pyroelectric data gathered on flux-grown crystals.

The pyroelectric figure of merit (p/K) for SbSI was computed from the pyroelectric coefficient p

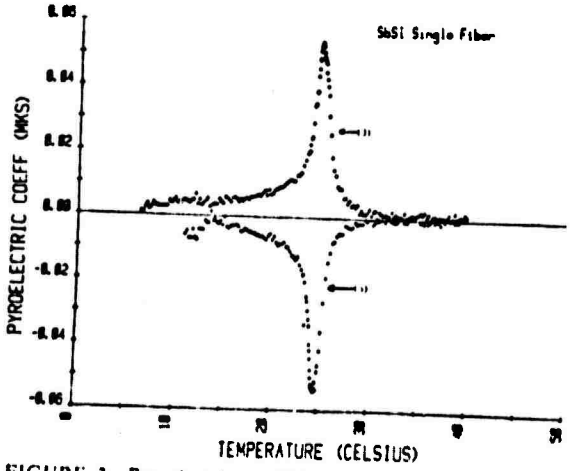

FIGURE 3 Pyroelectric coefficient of vapor grown SbSI crystal.

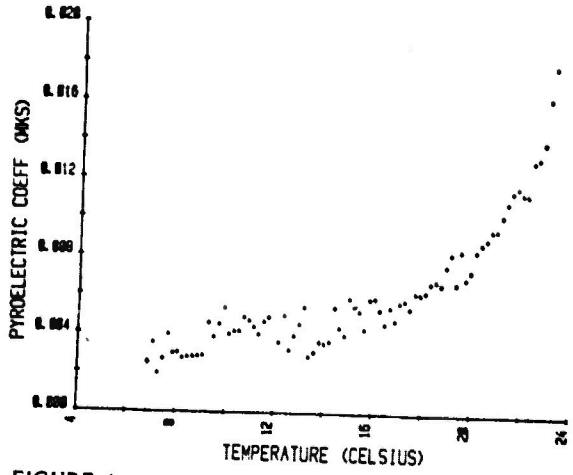

FIGURE 4 p vs T for the vapor grown SbSI single crystal fiber below the ferroelectric transition ($T_c \sim 24.7$°C).

and the dielectric constant K measured at various temperatures, and is plotted in Figure 6. From 5°C to about 20°C, p/K is 2×10^{-6} (MKS) but rises sharply to 10^{-5} at the transition, comparable to the TGS (1.1×10^{-5} MKS).

According to Devonshire's phenomenological theory of ferroelectricity, for a crystal in the stress-free state thermodynamic potential $A(P)$ can be expressed as

$$A(P) = A_0(T) + \frac{\beta}{2}(T-T_0)P^2 + \frac{rP^4}{4} + \frac{\delta P^6}{6} + \ldots \quad (2)$$

where P is the electric polarization and β, r, and δ are temperature-independent coefficients. Using

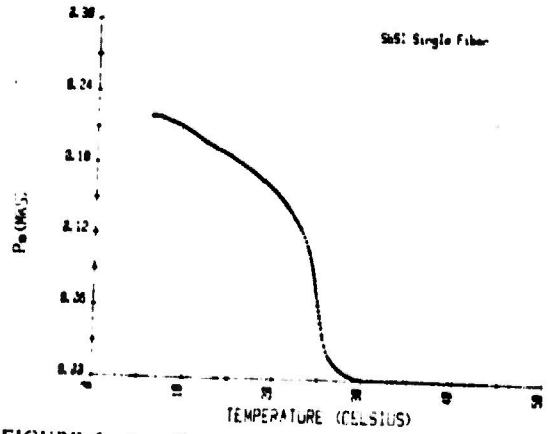

FIGURE 5 P_s vs T as calculated from the pyroelectric data.

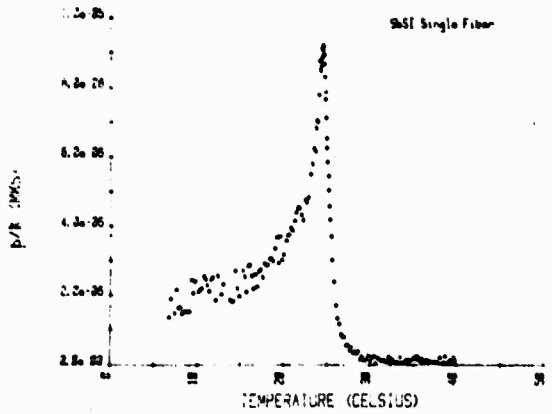

FIGURE 6 p/K as computed from the measured pyroelectric coefficient and the dielectric constant at various temperatures encompassing the phase transition.

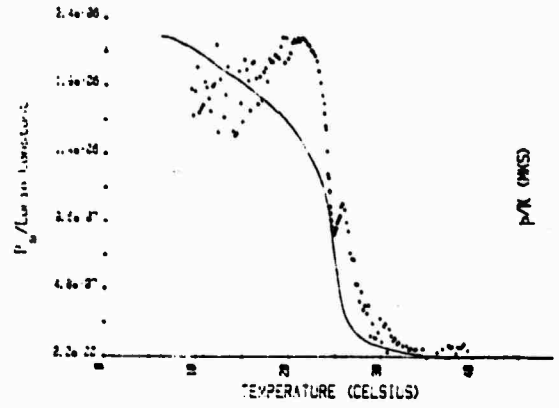

FIGURE 7 Plots of P_s/C and p/K vs temperature, after applying the isothermal correction to the dielectric constant.

only the second order terms, Liu and Zook[11] derived a relation

$$\frac{p}{K} = \frac{P_s}{C} \tag{3}$$

where C is the Curie constant and assumed to be temperature independent. Eq. (3) indicates that the figure of merit p/K should follow the slope of P_s vs T curve. The validity of this relation was tested on SBN using the Chynoweth method, and on TGS and DTGFB using an automated Byer-Roundy technique.[12] The experimental values and the theoretical predictions are in agreement over a temperature range 20°C below the transition in TGS and DTGFB.

It is clear from Figures 5 and 6 that $p/K(T)$ does not follow the temperature dependence of P_s. The discrepancy might be real, or it could arise from errors in the measured values of p and K. The spontaneous polarization P_s computed from the integration of p is in good agreement with the value obtained from the E-D curve supporting the validity of the pyroelectric coefficient measurements. This suggests the possibility of discrepancies in the dielectric constant. In the present set-up the dielectric constants at 1 MHz are not measured under steady-state conditions, and thus do not give the isothermal values needed to establish the validity of relation (3). The measured values are closer to the adiabatic dielectric permittivity. This suggests a correction to the measured permittivity based on the following relation.[13]

$$K_T = K_S + \frac{p^2 T}{\epsilon_0 c_p} \tag{4}$$

where K_T and K_S are the isothermal and adiabatic dielectric constants, and c_p is the volume specific heat of SbSI. Isothermal dielectric constants were calculated at various temperatures. A sharp dielectric anomaly representing the first order transition appears at 24.7°C. Revised plots of (p/K_T) vs T and (P_s/C) vs T are shown in Figure 7. Both functions show a sharp decrease near the Curie temperature, but some anomalies in p/K_T remain. Further study of the higher order terms in the Devonshire theory and of the temperature dependence of the property coefficients is needed.

The highest value of the figure of merit (p/K_T) is about 2.4×10^{-6} measured 5° below T_c.

ACKNOWLEDGEMENT

We wish to thank our colleagues at the Materials Research Laboratory for their advice and assistance. This work was sponsored by the Defense Advanced Research Projects Agency (Contract No. DARPA Project No. P-15124-MS).

REFERENCES

1. E. Fatuzzo, G. Harbeke, W. J. Merz, R. Nitsche, H. Roetchi and W. Ruppel, *Phys. Rev.*, **127**, 2036 (1962).
2. R. Nitsche and W. J. Merz, *J. Phys. Chem. Solids*, **13**, 154 (1960).
3. L. M. Belyaev, V. A. Lyakhovitskaya and I. M. Sil'vestrova, *Izv. Akad. Nauk SSSR. Neorgan. Mat.*, **6**, 429 (1970).
4. S S. Boksha, V. A. Lyakhovitskaya, I. M. Sil'vestrova and N. A. Tikhomirova, *Izv. Akad. Nauk SSSR, Neorgan. Mat.*, **6**, 1951 (1970).
5. E. Dönges, *Z. Anorg. Allgem. Chem.*, **263**, 112 (1950).
6. A. Kikuchi, Y. Oka and E. Sawaguchi, *J. Phys. Soc. Japan*, **23**, 337 (1967).

7. J. P. Dougherty and R. J. Seymour, *Rev. Sci. Inst.* (to be published).
8. R. L. Byer and C. B. Roundy, *Ferroelectrics*, **3**, 333 (1972).
9. A. S. Bhalla, K. E. Spear and L. E. Cross, *Mat. Res. Bull.*, **14**, 423 (1979).
10. K. Nassau, J. W. Shiever and M. Kowalchik, *J. Cryst. Growth*, **7**, 237 (1970).
11. S. T. Liu and J. D. Zook, *Ferroelectrics*, **7**, 171 (1974).
12. R. J. Seymour, J. P. Dougherty and A. Shaulov, *Phys. Rev. Lett.* (submitted).
13. M. E. Lines and A. M. Glass, *Principles and Applications of Ferroelectrics and Related Materials*, Clarendon Press, Oxford, 1977, p. 129.

APPENDIX VI

Primary and Secondary Pyroelectricity in Single Crystals of Antimony Sulphur Iodide

A. S. Bhalla

Primary and Secondary Pyroelectricity in Single Crystals of Antimony Sulphur Iodide

by

A.S. Bhalla

Antimony sulphur iodide is an interesting ferroelectric material with an extremely large dielectric and piezoelectric coefficients. It goes through a displacive first order transition at 20°C with large anomaly in the ferroelectric properties. In the ferroelectric phase it belongs to the orthrhombic mm2 point group symmetry and has large structural anisotropy along the polar c-axis. Thus it is difficult to grow the crystals with large cross-sectional area to make good electrical measurements. An empirical relationship based on the Devonshire's phenomenology of proper ferroelectrics predicts that the pyroelectric coefficients are directly related to the dielectric constants. This suggests that SbSI may have very high pyroelectric coefficients. Some reports on the large pyroelectric effect in SbSI have been made but no reliable measurements of the pyroelectric coefficient and its temperature dependance have been reported in the literature.

SbSI crystals are grown by the flux and the chemical vapor deposition methods. It is observed that the transition temperature of SbSI is sensitive to the impurities and thus affected by the growth method. The flux grown crystals have the transition ∿19°C where as in the vapor grown crystals Tc depends upon the impurity contents of sulphur, oxygen and antimony. The slight concentration of these impurities shifts the transition to the higher temperature side and affects the pyroelectric and dielectric properties. The relative effects on the pyroelectric properties have also been studied in this paper. The measurements of the pyroelectric coefficients are made by the automated set-up using the Byre-Roundy method.

Figure 1 shows the pyroelectric coefficient vs temperature on the vapor grown single crystal sample. The coefficients are unusually large even far below the Tc. Figure 2 shows the relative magnitude of the pyroelectric coefficient vs T in case of flux and vapor grown crystals. At 12°C the values of the pyroelectric coefficients are

$-5500\ \mu C/m^2{}^\circ C$ flux grown

$-3800\ \mu C/m^2{}^\circ C$ vapor grown

It is evident that the coefficients are very large as one expected from the large structural anisotropy present along the c-axis. The pyroelectric coefficients p_T are the sum of the primary and the secondary pyroelectricity. The secondary component is the product of thermal expansion, piezoelectric and elastic coefficients. Because of the unusually large piezoelectric ($\sim$2000 x 10^{-12}C/N at 12°C) and thermal expansion coefficient along c-axis ($\sim 10^{-4}/^\circ C$), a large secondary effect is expected in SbSI.

$$p_T^{E,\sigma} = p_{prim}^{\varepsilon} + d_{ijk}\ \alpha_{ij}\ C_{ijkl}^{E}$$

Unfortunately there is not enough data in the literature on the elastic coefficients of SbSI but reasonable data on α_{ij} and d_{33} are available. The piezoelectric coefficients d_{31} and d_{32}, are obtained from the inverse piezoelectric effect (i.e. by measuring the induced strain). The elastic constants C_{ij}^{D} have been recently reported by Sandercock. With the help of the measured coupling coefficients the values of C_{ij}^{E} were estimated. The most important coefficients in the calculations C_{33}^{E}, d_{33}^{E} and α's are taken from the measured values. From these numbers the rough estimation of the secondary pyroelectric effect in SbSI is made. The calculated secondary pyroelectricity is of the same order and of same sign as those experimentally measured total pyroelectric effect. Thus it suggests that the pyroelectricity in SbSI is largely due to the secondary effect which is pronounced because of its structural anisotropy.

Estimation of the secondary pyroelectricity in SbSI

C_{11}^D	3.06×10^{10} N/m^2	C_{11}^E	2.9×10^{10} N/m^2
C_{22}^D	3.14×10^{10} N/m^2	C_{22}^E	2.8×10^{10} N/m^2
C_{33}^D	5.18×10^{10} N/m^2	C_{33}^E	1.7×10^{10} N/m^2
C_{12}^D	0.85×10^{10} N/m^2	C_{12}^E	0.6×10^{10} N/m^2
C_{13}^D	0.97×10^{10} N/m^2	C_{13}^E	0.9×10^{10} N/m^2
C_{23}^D	1.44×10^{10} N/m^2	C_{23}^E	1.3×10^{10} N/m^2
k_{33}	0.8	α_1	-0.4×10^{-4}/°C
k_{31}	0.3	α_2	1.1
k_{32}	0.3	α_3	-2.5
		d_{31}	143×10^{-12} C/N
		d_{32}	-650×10^{-12} C/N
		d_{33}	2130×10^{-12} C/N

$$(p_3)_{sec} = d_{3i}\, C_{ij}\, \alpha_j \qquad i,j = 1\text{-}3$$
$$\simeq -7000\ \mu C/m^2{}^\circ C$$

The total pyroelectricity measured at 12°C $\simeq -6000\ \mu C/m^2{}^\circ C$. Thus there is a major contribution from the secondary pyroelectricity to the total pyroelectric effect in SbSI single crystals. The sign of the secondary pyroelectricity is negative and the magnitude of the effect is comparable to the total effect. In proper ferroelectrics no such case is reported where the pyroelectricity is dominated by the secondary pyroelectric effect in a crystal. Since in the present case secondary effect is calculated from the estimated C_{ij}^E coefficients, a more accurate measurements are needed to understand the origin of pyroelectricity in SbSI.

If the secondary effect is truly dominating the pyroelectricity in SbSI, in that case the oblique cut in this material should give a large enhancement in p/K figure of merit. SbSI has a very large anisotropy in dielectric properties where as d, α and c will still be large enough to give a substantial secondary effect in an oblique cut SbSI single crystal.

References

Scielding, C. and Schmidt, G., Phys. Stat. Sol. (a) 9, K77 (1972).

Sandercock, J. R., Opt. Commun. 2, 73 (1970).

Nassau, K., Shiever, J. W., Kowalchik, M., J. Cryst. Growth 7, 237 (1970).

Bhalla, A. S., Spear, K. E. and Cross, L. E., Mat. Res. Bull. 14, 423 (1979).

Bhalla, A. S. and Newnham, R. E., Phys. Stat. Solidi (a) 58, K19 (1980).

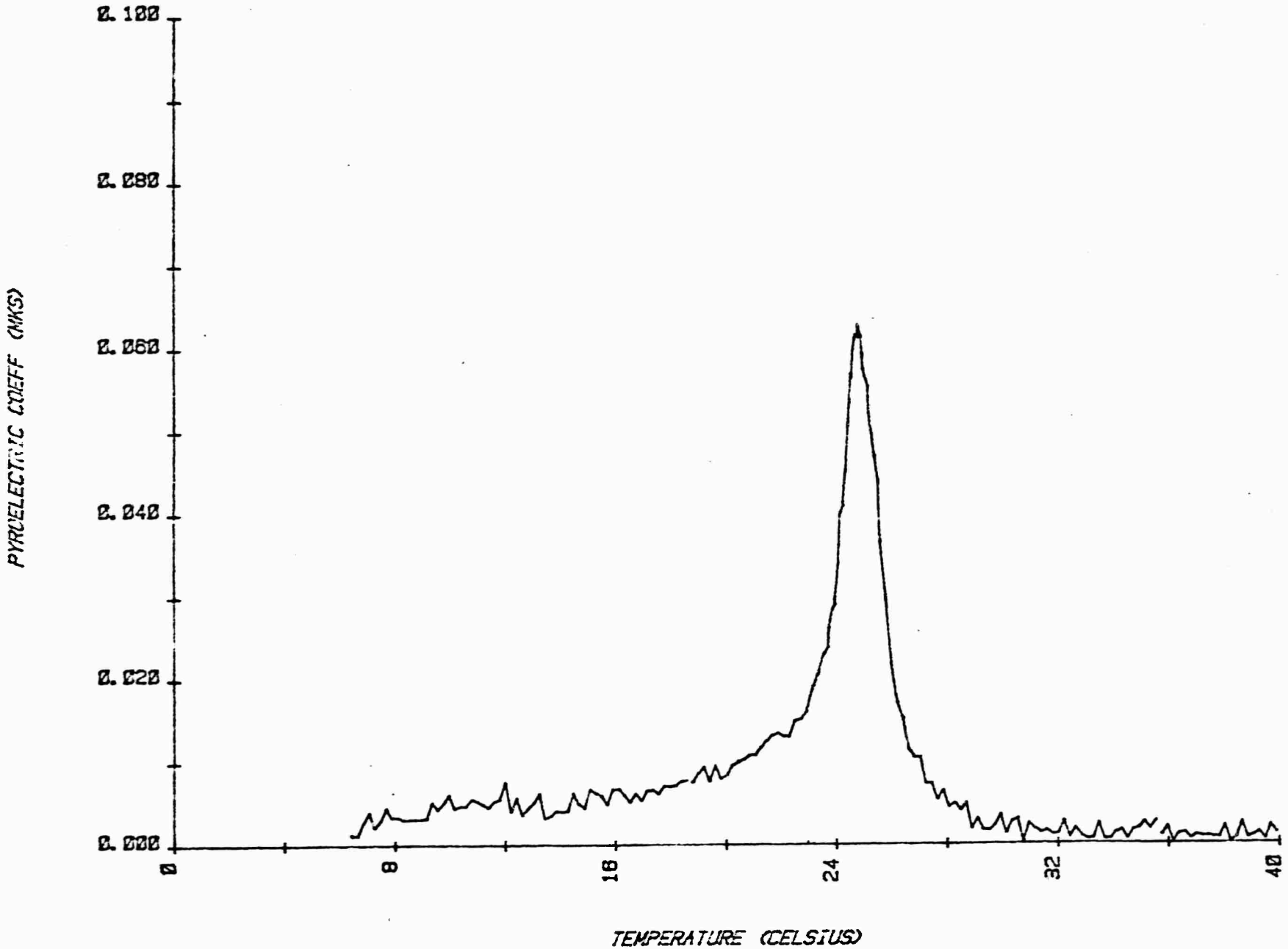
0.100
0.080
0.060
0.040
0.020
0.000
PYROELECTRIC COEFF (MKS)
0
8
16
24
32
40
TEMPERATURE (CELSIUS)

Figure 1

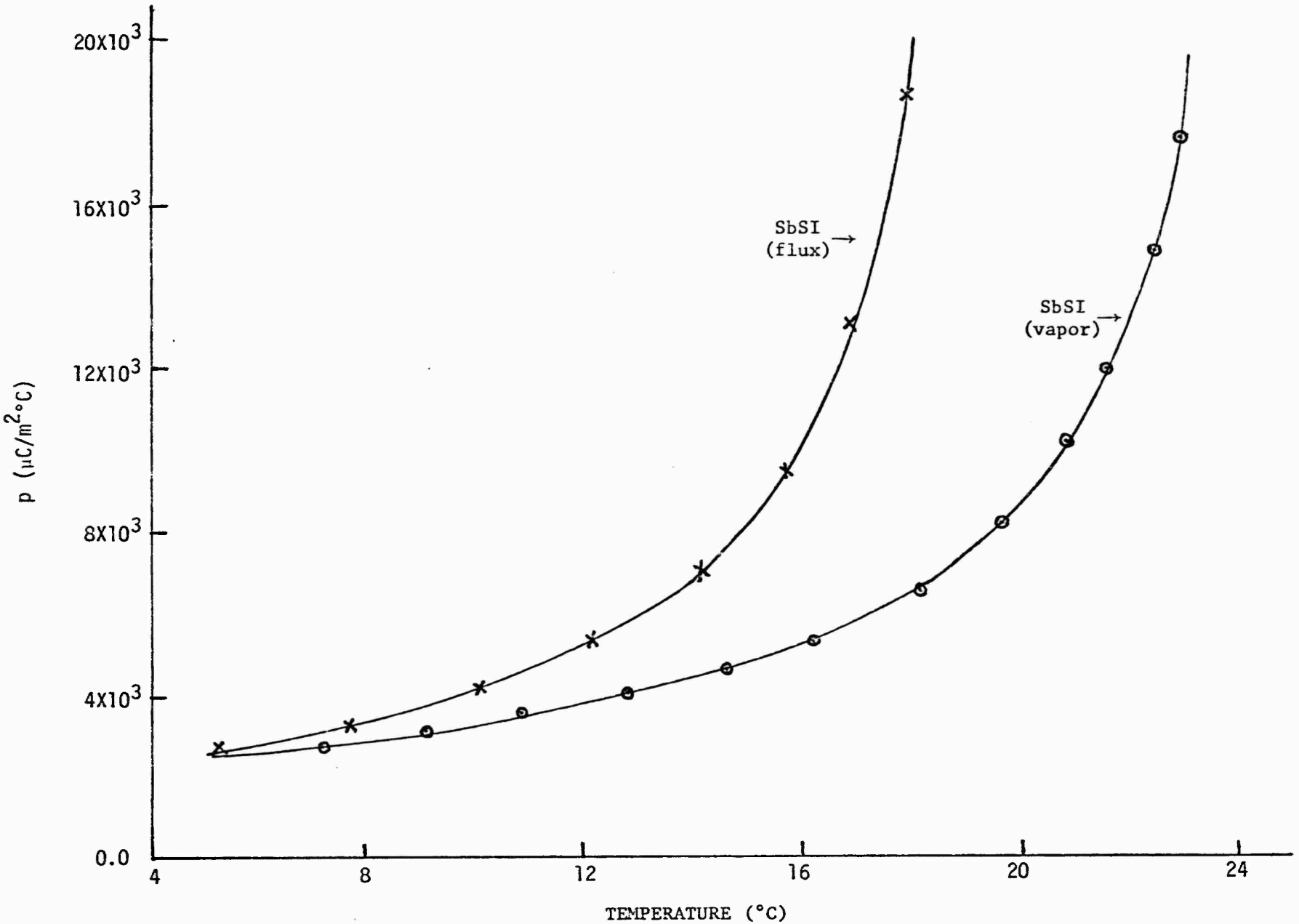
20X10^3
16X10^3
12X10^3
8X10^3
4X10^3
0.0
p (μC/m^2°C)
SbSI (flux)
SbSI (vapor)
4
8
12
16
20
24
TEMPERATURE (°C)

Figure 2

APPENDIX VII

Paper Presented at the ACA Meeting, August 1980, Canada

HOLEY CRYSTALS*. R. E. Newnham and A. S. Bhalla, Materials Research Laboratory, Pennsylvania State University, University Park, Pennsylvania 16802.

Single crystals containing minute interconnected channels have a number of unusual properties such as low density, machinability, and high surface area. The possibility of incorporating a second phase (gas, liquid, or solid) in such crystals suggests some interesting applications; examples drawn from materials science, mineralogy, and medicine will be discussed. During the past several years we have been exploring techniques for making holey crystals; methods based on a lost wax process utilizing a disposable second phase are especially interesting. Coral is sometimes used as a starting pattern. Because of the unusual flux paths involved, holey ferroelectric and ferromagnetic crystals can be poled in several directions simultaneously, offering some novel transducer configurations. Single crystal SbSI - silica fiber composites for pyroelectric and optical applications were grown by the Czochralski method.

*Research sponsored by Advanced Research Projects Agency under Contract MDA-78-C-0306.